NASA MEMO 10-3-58L

NASA MEMORANDUM

WIND-TUNNEL INVESTIGATION OF SOME EFFECTS OF WING SWEEP AND HORIZONTAL-TAIL HEIGHT ON THE STATIC STABILITY OF AN AIRPLANE MODEL AT TRANSONIC SPEEDS

By Lewis R. Fisher and James L. Williams

Langley Research Center
Langley Field, Va.

NATIONAL AERONAUTICS AND SPACE ADMINISTRATION
WASHINGTON
October 1958
Declassified April 12, 1961

NATIONAL AERONAUTICS AND SPACE ADMINISTRATION

NASA MEMO 10-3-58L

WIND-TUNNEL INVESTIGATION OF SOME EFFECTS OF WING SWEEP AND HORIZONTAL-TAIL HEIGHT ON THE STATIC STABILITY OF AN AIRPLANE MODEL AT TRANSONIC SPEEDS*

By Lewis R. Fisher and James L. Williams

SUMMARY

A research model of an airplane with a configuration suitable for supersonic flight was tested at transonic speeds in order to establish the effects on longitudinal and lateral stability of certain changes in both wing sweep and height of the horizontal tail. Two wings of aspect ratio 3 and taper ratio 0.15, one having the quarter-chord line swept back 30° and the other 45°, were each tested with the horizontal tail of the model in a low and in a high position. One configuration was also tested with fuselage strakes. The tests were made at Mach numbers from 0.60 to 1.17 and Reynolds numbers from 1.9×10^6 to 2.6×10^6.

The results indicated that a low horizontal-tail position (below the wing-chord plane) gave positive longitudinal stability for the model for all angles of attack used (angles of attack up to 24°); whereas, a higher tail position (above the wing-chord plane) resulted in a large reduction in stability at moderate angles of attack. With the higher horizontal tail, the 30°-swept-wing model had somewhat more stability than the 45°-swept-wing model at subsonic Mach numbers. With the lower tail, the 45°-swept-wing model had slightly more stability at all Mach numbers.

The model with the 30° swept wing had greater directional stability with the tail in the higher rather than the lower position, but the opposite was true for the 45°-swept-wing model. The directional stability decreased sharply at high angles of attack; this characteristic was alleviated by the use of fuselage strakes which, however, proved to be detrimental to the longitudinal stability of the model tested.

*Title, Unclassified.

INTRODUCTION

The geometric features of an airplane configuration, such as wing sweep and low aspect ratio, which make it suitable for supersonic flight very often result in certain adverse stability characteristics in the form of losses in longitudinal or directional stability for the airplane in the transonic flight regime. In the present investigation an airplane configuration was tested through the transonic speed range in order to determine the effects of certain changes in wing sweep and in horizontal-tail height on the static lateral and longitudinal stability of the model.

In the investigation of reference 1 fuselage strakes are shown to be a device which, at high subsonic speeds, reduces the directional instability of a wing-fuselage combination at high angles of attack and thereby results in a considerable improvement in the directional stability of the complete airplane configuration. One model configuration was tested with strakes in the present investigation in order to see whether a similar improvement can be gained at transonic speeds.

SYMBOLS

All forces and moments were measured in the system of body axes shown in figure 1 with the origin of the axis system located at the mean aerodynamic quarter-chord line projected to the plane of symmetry. The data presented herein are in the form of lift, drag, and pitching-moment coefficients in the system of stability axes (fig. 1) and the rolling-moment, yawing-moment, and lateral-force coefficients in the system of body axes. The symbols and coefficients are defined as follows:

b	wing span, ft
c	wing chord, ft
$\bar{c}$	wing mean aerodynamic chord, $\frac{2}{S}\int_0^{b/2} c^2 dy$, ft
M	Mach number
q	free-stream dynamic pressure, lb/sq ft
R	Reynolds number
S	wing area, sq ft

y spanwise station, ft

α angle of attack, deg

β angle of sideslip, deg

C_L lift coefficient, $\frac{\text{Lift}}{qS}$

$C_{D'}$ component of drag coefficent along X stability axis

C_Y lateral-force coefficient, $\frac{\text{Lateral force}}{qS}$

C_l rolling-moment coefficient, $\frac{\text{Rolling moment}}{qSb}$

C_m pitching-moment coefficient, $\frac{\text{Pitching moment}}{qS\bar{c}}$

C_n yawing-moment coefficient, $\frac{\text{Yawing moment}}{qSb}$

$C_{l_\beta} = \frac{\partial C_l}{\partial \beta}$

$C_{n_\beta} = \frac{\partial C_n}{\partial \beta}$

$C_{Y_\beta} = \frac{\partial C_Y}{\partial \beta}$

Model designations:

$W_{30}F$ 30° swept wing, fuselage

$W_{30}FT_H$ 30° swept wing, fuselage, vertical tail, ventral fin, high horizontal tail

$W_{30}FT_L$ 30° swept wing, fuselage, vertical tail, ventral fin, low horizontal tail

$W_{45}F$ 45° swept wing, fuselage

$W_{45}FT_H$ 45° swept wing, fuselage vertical tail, ventral fin, high horizontal tail

$W_{45}FT_L$ 45° swept wing, fuselage, vertical tail, ventral fin, low horizontal tail

MODELS AND APPARATUS

A sketch of the models used in the present investigation is presented in figure 2, and additional geometric characteristics are presented in table I. The mid-wing, fuselage-tail configuration was designed so that the wing and tails were removable in order to permit tests of the model components in various combinations. Except for the wings, the model used was the same as the one used in the investigation of reference 2.

The fuselage had an overall fineness ratio of about 11 and was a body of revolution made up of a 3.5-fineness-ratio ogive nose, a cylindrical center section, and a boattailed rear section. Two wing plan forms were used in this investigation, one having a quarter-chord sweep of 30° and the other a sweep of 45°. Both wings had an aspect ratio of 3, a taper ratio of 0.15, and NACA 65A004 airfoil sections parallel to the plane of symmetry. The model was equipped with a ventral fin and a vertical tail having a wedge leading edge of 45° semi-vertex angle and a slab side of constant thickness. Two horizontal-tail locations were used: (1) a low tail position wherein the horizontal tail was located on the ventral fin below the wing-chord plane, and (2) a high tail position wherein the tail was located at about the 60-percent-span height of the vertical tail.

The 30°-swept-wing high-tail model configuration was tested with fuselage strakes which extended around the nose and from the nose to the juncture of the wing leading edge with the fuselage. These strakes projected 0.2 inch from the fuselage and were 0.031 inch in thickness as shown in figure 2.

The model was mounted on a sting support by means of an internal six-component electrical strain-gage balance in the Langley 8-foot transonic tunnel. (See fig. 3.) This wind tunnel is a dodecagonal, slotted-throat, single-return tunnel operating at atmospheric stagnation pressures and stagnation temperatures between 80° F and 180° F and was designed for obtaining aerodynamic data through the speed of sound without the usual effects of choking and blockage. A complete description of the tunnel can be found in reference 3.

TESTS

The model was tested through the transonic speed range from $M = 0.60$ to $M = 1.17$ with both the 30° swept wing and the 45° swept wing. With

each wing tests were made with the horizontal tail in both the low and the high vertical position and with the tail surfaces, including the vertical tail and the ventral fin, completely off. In addition the 30°-swept-wing, high-horizontal-tail configuration was tested with strakes.

The tests were made for a range of angles of attack from approximately 0° to 24° for each configuration and Mach number and at sideslip angles of 0° and ±6°. The quantities measured were normal, axial, and lateral forces, pitching, yawing, and rolling moments, and base pressures. In addition, the 30°-swept-wing, high-tail configuration was tested at $\alpha = 6^\circ$ for a sideslip angle range from -4° to 20°. Data were not measured over the complete angle-of-attack and angle-of-sideslip ranges for some of the higher Mach numbers because of the load limits imposed on the balance.

The Reynolds number based on the wing mean aerodynamic chord varied from about 1.94×10^6 to 2.61×10^6. The variation of Reynolds number with Mach number is presented in figure 4.

CORRECTIONS

No corrections to the free-stream Mach number and dynamic pressure for the effects of model and wake blockage are necessary for tests made in the slotted test section of the Langley 8-foot transonic tunnel (ref. 4). No test data were taken in the Mach number range ($1.03 < M < 1.12$) where the reflected boundary disturbance impinged upon the model.

The axial-force data, before being resolved into drag, have been adjusted in such a manner that the axial force corresponds to the condition where the base pressure is equal to the free-stream static pressure. No corrections for the forces and moments produced by sting interference have been applied to the data. It is indicated in reference 5 that the significant corrections would be limited to small increments in pitching moment and drag for the ratio of sting cross-sectional area to model base area of 0.56 employed herein. Corrections to angle of attack and angle of sideslip due to support-system deflections under load were found to be negligible.

RESULTS AND DISCUSSION

Longitudinal Stability Characteristics

The longitudinal aerodynamic coefficients for the model with each of two wings and two horizontal tail heights for each wing are shown in figure 5. The lift and drag coefficients are presented without discussion;

a few remarks are made which are pertinent to the static stability in pitch.

For the horizontal tail in the relatively high position the model with either the 30° or 45° swept wing suffered a decrease in longitudinal stability at an angle of attack between 8° and 12° depending upon Mach number. For $M < 0.98$, the 30°-swept-wing model exhibited somewhat better stability characteristics than did the 45°-swept-wing model for the high tail position in the high angle-of-attack region. With the horizontal tail in the low position, the model with either wing was generally stable throughout the angle-of-attack range for each Mach number. The 45°-swept-wing model had slightly more stability than the 30°-swept-wing model at low angles of attack and more negative pitching moments at all angles of attack.

Figure 6 presents the longitudinal coefficients for the 30°- and 45°-swept-wing—fuselage combinations without the vertical and horizontal tail surfaces and without the ventral fin. The longitudinal stability for the model with each wing increased as the Mach number increased from $M = 0.60$ to $M = 0.98$ and remained relatively constant from $M = 0.98$ to $M = 1.17$. The 45°-swept-wing model exhibited somewhat more longitudinal stability through the Mach number range than did the 30°-swept-wing model. The difference in the stability shown by the two wings in figure 6 being approximately the same as the difference shown between the two wings in the presence of the tail surfaces as shown in figure 5 indicates that this increase in longitudinal stability for the 45° swept wing is a direct effect of wing sweep.

The 30°-swept-wing, high-tail configuration was tested with fuselage strakes. The use of strakes generally alleviates the directional stability deficiencies that occur at high angles of attack (refs. 1 and 6). The effect of the strakes on the longitudinal stability for the configurations tested is shown in figure 7. The use of strakes led to a severe reduction in the longitudinal stability of both the tail-on and tail-off configurations at all Mach numbers and angles of attack. As is shown in reference 1, however, the reduction in longitudinal stability can be minimized by the proper selection of the shape of the strakes. It is also pointed out in this reference, if a horizontal-tail location is selected such that the configuration is characterized by increasing stability with angle of attack, then the model can still have acceptable stability despite the addition of fuselage strakes with their inherent tendency to reduce the longitudinal stability.

Lateral-Stability Characteristics

The effect of horizontal-tail height on the lateral stability derivatives for the complete-model configurations with either wing is presented

in figure 8. With reference to the 30°-swept-wing model, the high horizontal-tail position resulted in somewhat more directional stability $\left(C_{n_\beta}\right)$ for $M > 0.95$ than did the low position through the angle-of-attack range. The opposite effect was shown for the 45°-swept-wing model in that the low tail position resulted in more directional stability than did the high position for all Mach numbers. With either wing, the model had greater effective dihedral $\left(-C_{l_\beta}\right)$ for the horizontal tail in the high rather than in the low position. For all configurations considered, the data show a sharp reduction in directional stability at the higher angles of attack primarily, it is subsequently shown, as a result of a decrease in the tail contribution to C_{n_β} with increasing angle of attack. It may be noted in figure 8 that the lateral force due to sideslipping $\left(C_{Y_\beta}\right)$ suffers a reduction at high angles of attack in a manner similar to that of C_{n_β}.

The lateral stability characteristics for the same configurations are shown as functions of Mach number in figure 9 for four angles of attack. The increment in Mach number between $M = 0.9$ to $M = 1.0$ is marked by large increases in the directional stability and effective dihedral derivatives, particularly at high angles of attack. At the higher Mach numbers, these derivatives generally tended to approach their subsonic values. The greatest overall changes in the lateral stability were shown by the models with the high horizontal tail.

The lateral stability characteristics of the wing-fuselage configuration is shown for the 30°-swept-wing model in figure 10 and the 45°-swept-wing model in figure 11. Except possibly for the lowest two or three Mach numbers, the C_{n_β} for the tail-off configurations is relatively constant with angle of attack; therefore, the reduction in C_{n_β} suffered by the complete model is primarily a result of a decrease in the tail contribution to C_{n_β} with increasing angle of attack.

For the tail-off configuration it is indicated in figure 12 that the 30°-swept-wing model had a lesser degree of directional instability than did the 45°-swept-wing model at high angles of attack.

The effect of fuselage strakes on the lateral stability derivatives for the 30°-swept-wing, tail-off and high-tail configurations are shown in figure 13. The use of strakes clearly led to a significant increase in the directional stability of both the tail-off and tail-on configurations at high angles of attack throughout the transonic Mach number range. The discussion in reference 1 indicates that the strakes accomplish this improvement in directional stability primarily by an alteration of the flow about the fuselage such that the unstable contribution of the fuselage to C_{n_β} is decreased. Figure 13 shows such an increase in the C_{n_β}

of the wing-fuselage combination caused by the strakes, but this increase is not sufficient to explain the increase in C_{n_β} for the complete model. The effectiveness of the vertical tail, possibly in combination with a more favorable pattern of wing-fuselage interference, is apparently increased as well by the use of strakes in this instance.

The results in figure 13 indicate that the fuselage strakes also increase the effective dihedral and lead to a large positive increment in the lateral force due to sideslipping for both the tail-on and tail-off configurations at high angles of attack.

Representative variations of the lateral force and moment coefficients with angle of sideslip for the 30°-swept-wing, high-tail configuration for $\alpha = 6^\circ$ are shown in figure 14. These coefficients were relatively linear and showed positive directional stability for the model up to at least the sideslip angle $\beta = 8^\circ$. For sideslip angles $\beta > 10^\circ$ the model demonstrated approximately neutral directional stability at all but the lowest Mach number.

CONCLUSIONS

A wind-tunnel investigation was conducted at transonic speeds to study the effects of certain changes in wing sweep and horizontal-tail height on the static stability characteristics of an airplane model. The two wings tested had respective sweep angles of 30° and 45° of the quarter-chord line. The horizontal tail was tested in a high position at 60 percent of the span of the vertical tail and at a point below the wing-chord plane on a ventral fin. The results of this investigation indicate the following conclusions:

1. The lower horizontal-tail location offered positive longitudinal stability throughout the Mach number and angle-of-attack ranges at which tests were made. The higher tail position resulted in a decrease of longitudinal stability at moderate angles of attack.

2. With the horizontal tail in the higher position, the 30°-swept-wing model exhibited somewhat better longitudinal stability characteristics than did the 45°-swept-wing model for only the subsonic Mach numbers. With the tail in the lower position, the 45°-swept-wing model had slightly more stability at low angles of attack than did the 30°-swept-wing model through the transonic speed range.

3. With the 30° swept wing the model had more directional stability at the higher Mach numbers with the tail in the higher rather than in the lower position. The opposite was true at all Mach numbers for the

45°-swept-wing model. The directional stability of each configuration tested decreased sharply at the higher angles of attack throughout the Mach number range.

4. The model with the higher tail position offered more effective dihedral than did the model with the lower tail position for either wing sweep.

5. The use of fuselage strakes resulted in a considerable improvement in the directional stability at high angles of attack of the test configurations at the transonic Mach numbers. This improvement, however, was accompanied by a detrimental effect of the strakes on the longitudinal stability of the model tested.

6. The models with the higher horizontal tail rather than the lower tail exhibited the greater overall changes in the lateral stability derivatives in the transonic Mach number range.

Langley Research Center,
National Aeronautics and Space Administration,
Langley Field, Va., July 8, 1958.

REFERENCES

1. Polhamus, Edward C., and Spreemann, Kenneth P.: Effect at High Subsonic Speeds of Fuselage Forebody Strakes on the Static Stability and Vertical-Tail-Load Characteristics of a Complete Model Having a Delta Wing. NACA RM L57K15a, 1958.

2. Spearman, M. Leroy, and Robinson, Ross B.: Investigation of the Aerodynamic Characteristics in Pitch and Sideslip of a 45° Swept-Wing Airplane Configuration With Various Vertical Locations of the Wing and Horizontal Tail - Static Lateral and Directional Stability; Mach Numbers of 1.41 and 2.01. NACA RM L57J25a, 1957.

3. Wright, Ray H., and Ritchie, Virgil S.: Characteristics of a Transonic Test Section With Various Slot Shapes in the Langley 8-Foot High-Speed Tunnel. NACA RM L51H10, 1951.

4. Wright, Ray H., and Ward, Vernon G.: NACA Transonic Wind-Tunnel Test Sections. NACA Rep. 1231, 1955. (Supersedes NACA RM L8J06.)

5. Osborne, Robert S.: High-Speed Wind-Tunnel Investigation of the Longitudinal Stability and Control Characteristics of a $\frac{1}{16}$-Scale Model of the D-558-2 Research Airplane at High Subsonic Mach Numbers and at a Mach Number of 1.2. NACA RM L9C04, 1949.

6. Sleeman, William C., Jr.: Investigation at High Subsonic Speeds of the Effects of Various Horizontal Fuselage Forebody Fins on the Directional and Longitudinal Stability of a Complete Model Having a 45° Sweptback Wing. NACA RM L56J25, 1957.

TABLE I.- GEOMETRIC CHARACTERISTICS OF MODELS

Wing:	
Sweep of quarter-chord line, deg	30 and 45
Area, sq in.	128
Span, in.	19.6
Root chord, in.	11.35
Tip chord, in.	1.70
Taper ratio	0.15
Aspect ratio	3
Mean aerodynamic chord, in.	7.71
Spanwise location of mean aerodynamic chord, in.	3.69
Airfoil section, parallel plane of symmetry	NACA 65A004
Horizontal tail:	
Area, sq in.	28.6
Span, in.	10.74
Root chord, in.	3.35
Tip chord, in.	2.01
Taper ratio	0.6
Aspect ratio	4
Sweep of quarter-chord line, deg	45
Tail height:	
Low position below wing-chord plane, in.	2.50
High position above wing-chord plane, in.	4.58
Airfoil section, parallel to plane of symmetry	NACA 65A006
Vertical tail:	
Area to body center line, sq in.	43.5
Span from body center line, in.	7.48
Root chord, in.	8.17
Tip chord, in.	3.44
Taper ratio	0.42
Aspect ratio	1.29
Sweep leading-edge, deg	35
Airfoil section	Wedge nose, slab side with constant thickness of 0.437 in.
Ventral fin:	
Exposed area, sq in.	8.54
Tip chord, in.	3.25
Sweep of leading edge, deg	70.1
Body:	
Length, in.	36.50
Diameter (maximum), in.	3.33
Diameter (base), in.	2.67
Length to diameter (ratio)	10.96

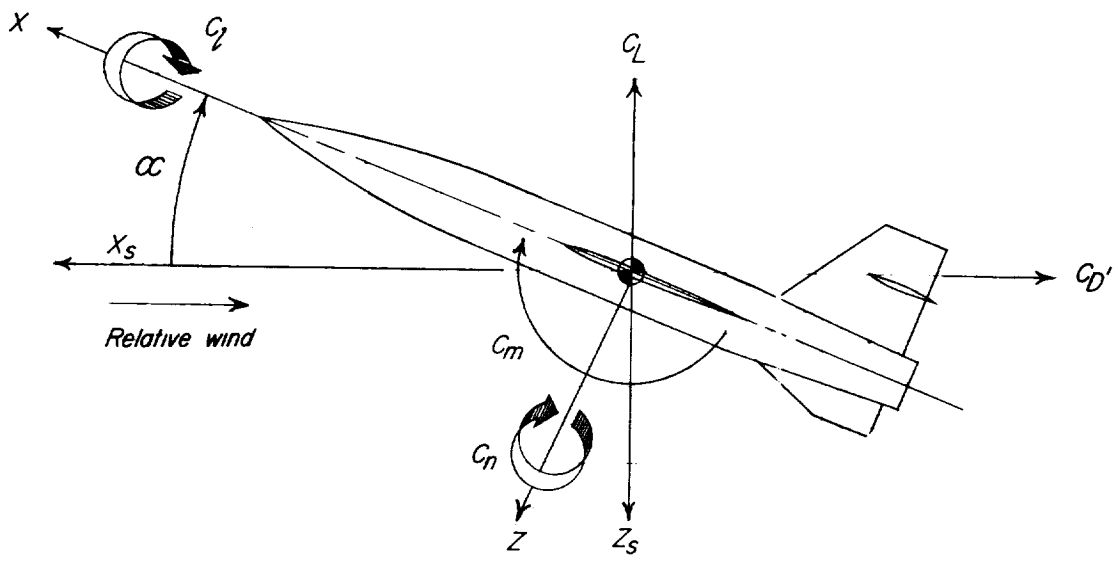

View A-A

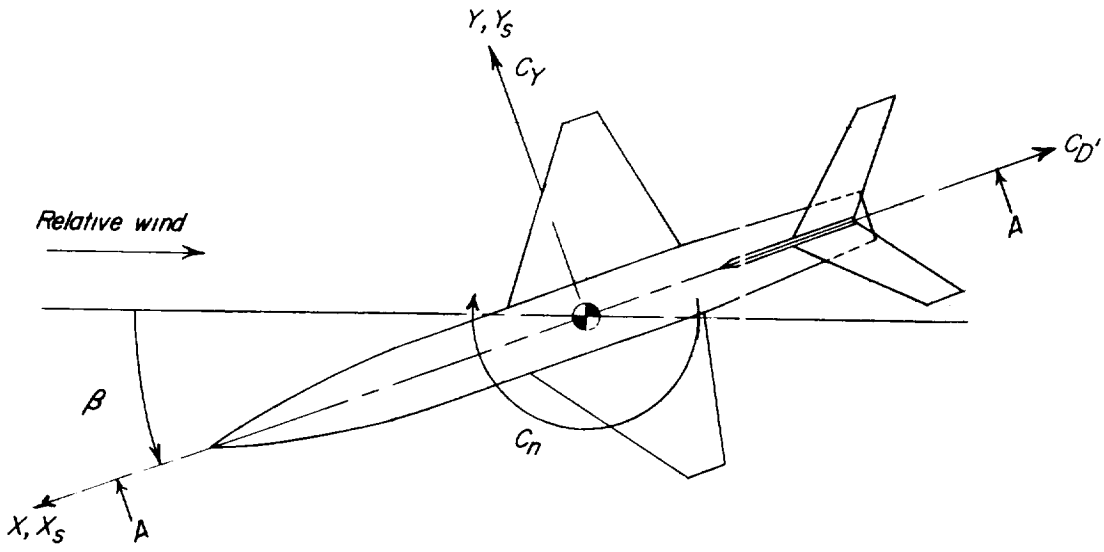

Figure 1.- Systems of axes. Arrows indicate positive directions of forces, moments, and angular displacements.

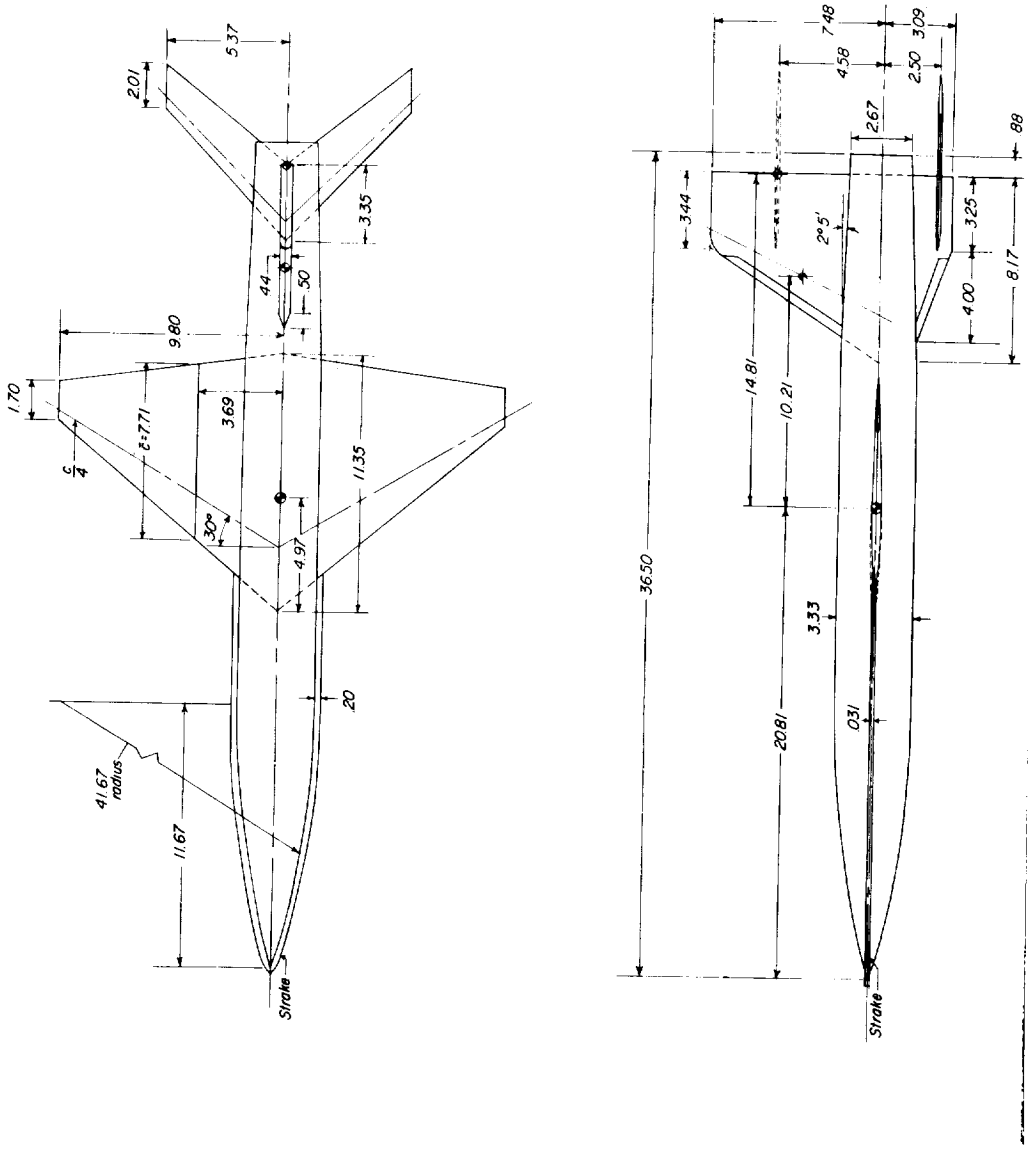

(a) Model with 30° sweptback wing.

Figure 2.- Configurations of models tested. Linear dimensions are in inches.

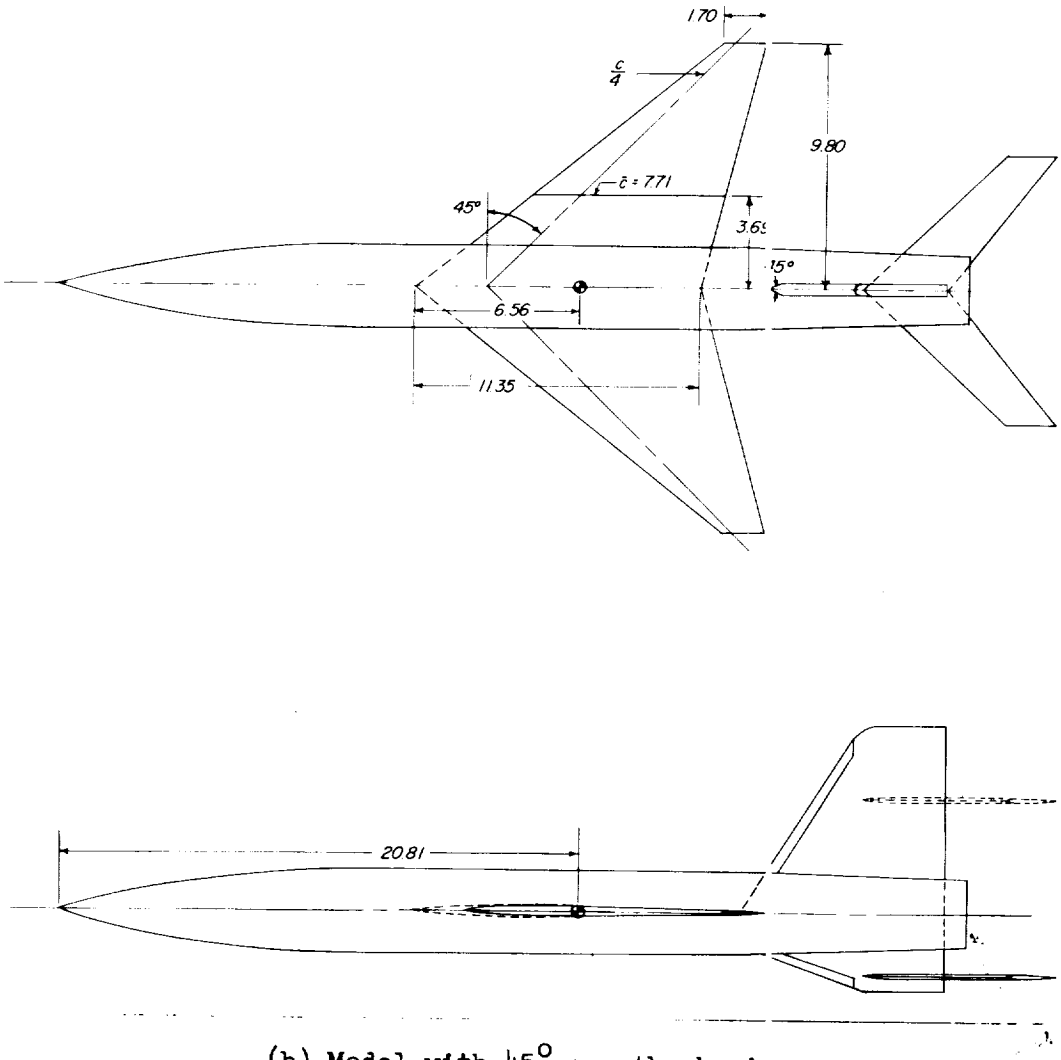

(b) Model with 45° sweptback wing.

Figure 2.- Concluded.

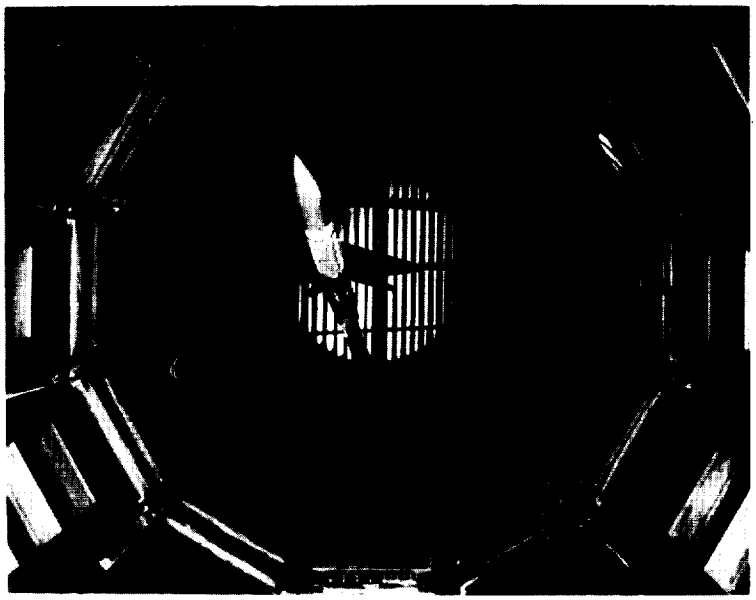

(a) $\alpha = 24^{\circ}$. L-57-2508

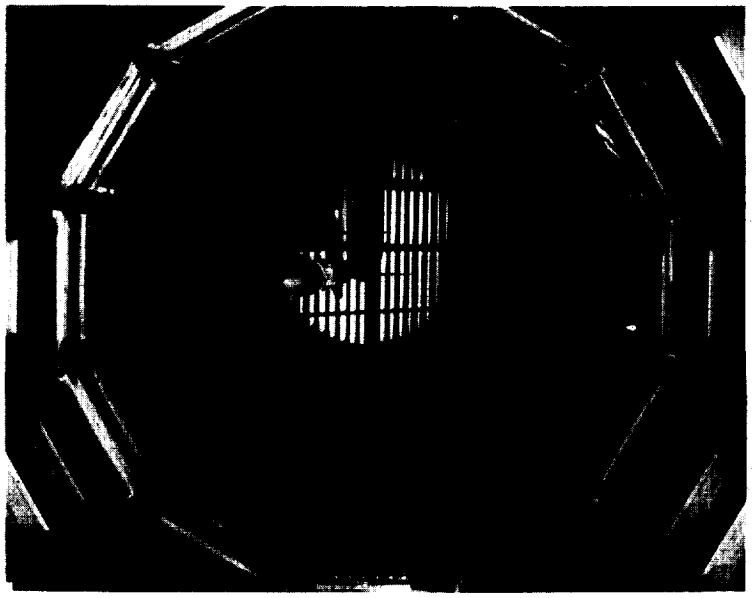

(b) $\alpha = 0^{\circ}$. L-57-2510

Figure 3.- The model with the 30° sweptback wing and the high horizontal tail mounted in the test section of the Langley 8-foot transonic tunnel. $\beta = -6^{\circ}$.

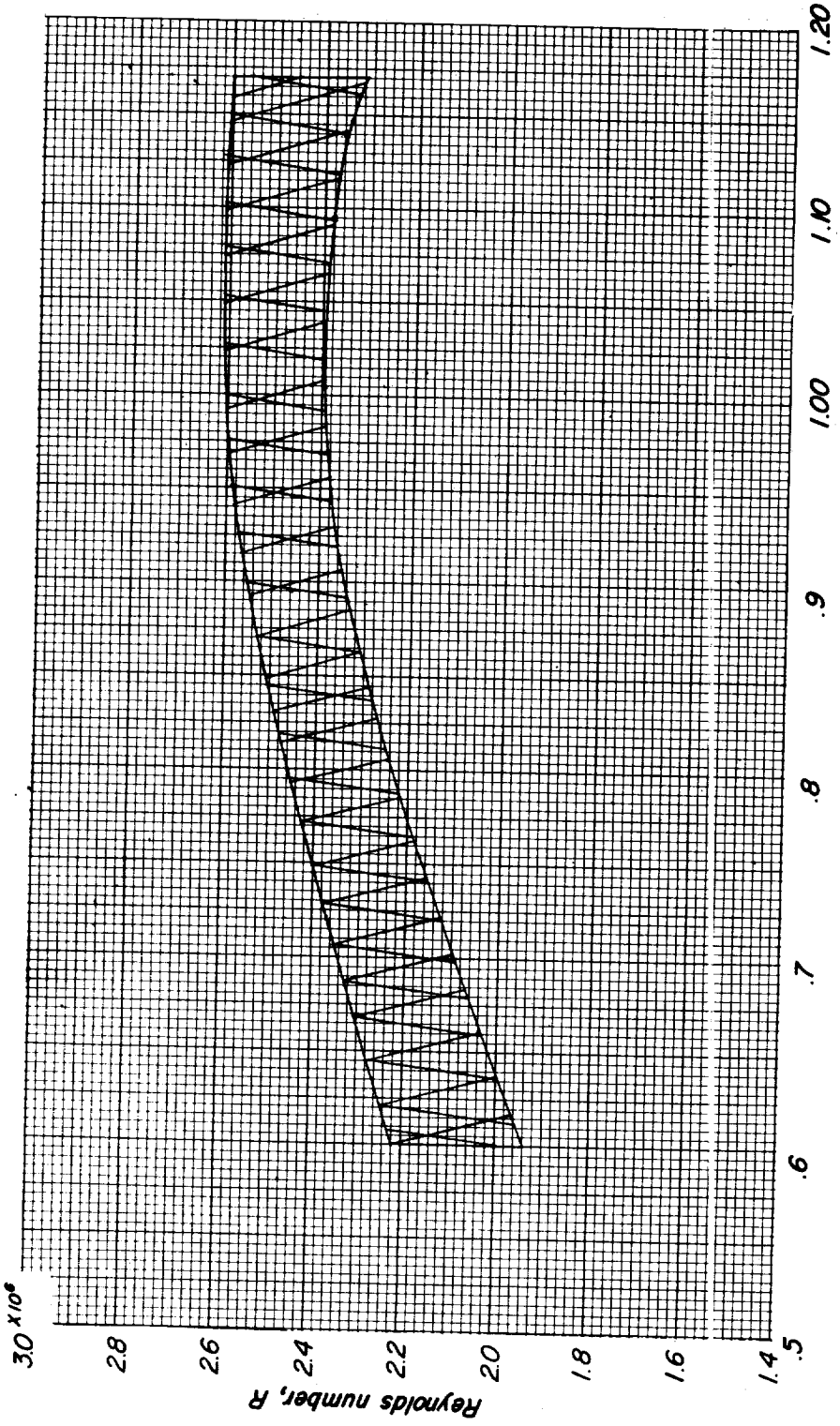

Figure 4.- Variation of Reynolds number (based on wing mean aerodynamic chord) with Mach number.

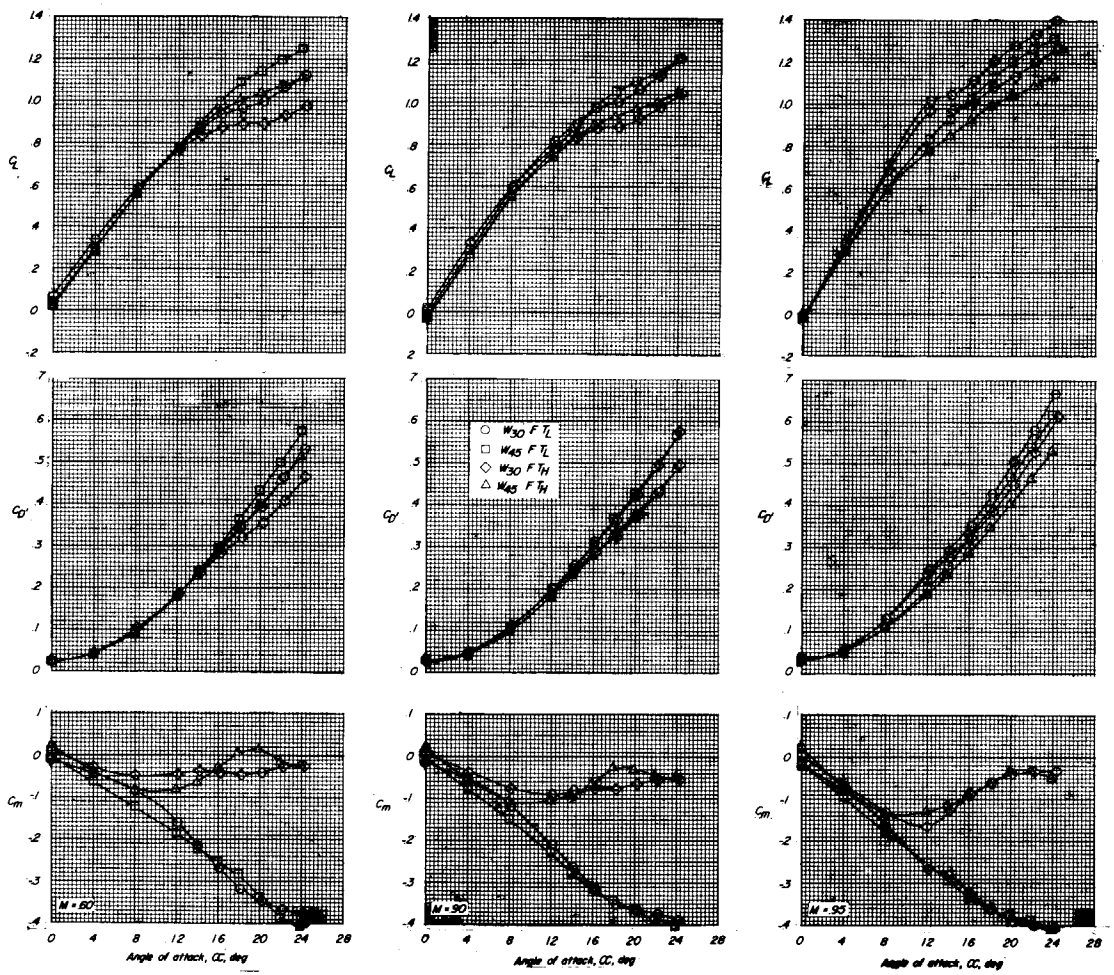

(a) M = 0.60. (b) M = 0.90. (c) M = 0.95.

Figure 5.- Variation with angle of attack of longitudinal aerodynamic coefficients for the model showing the effect of wing sweepback and horizontal-tail height.

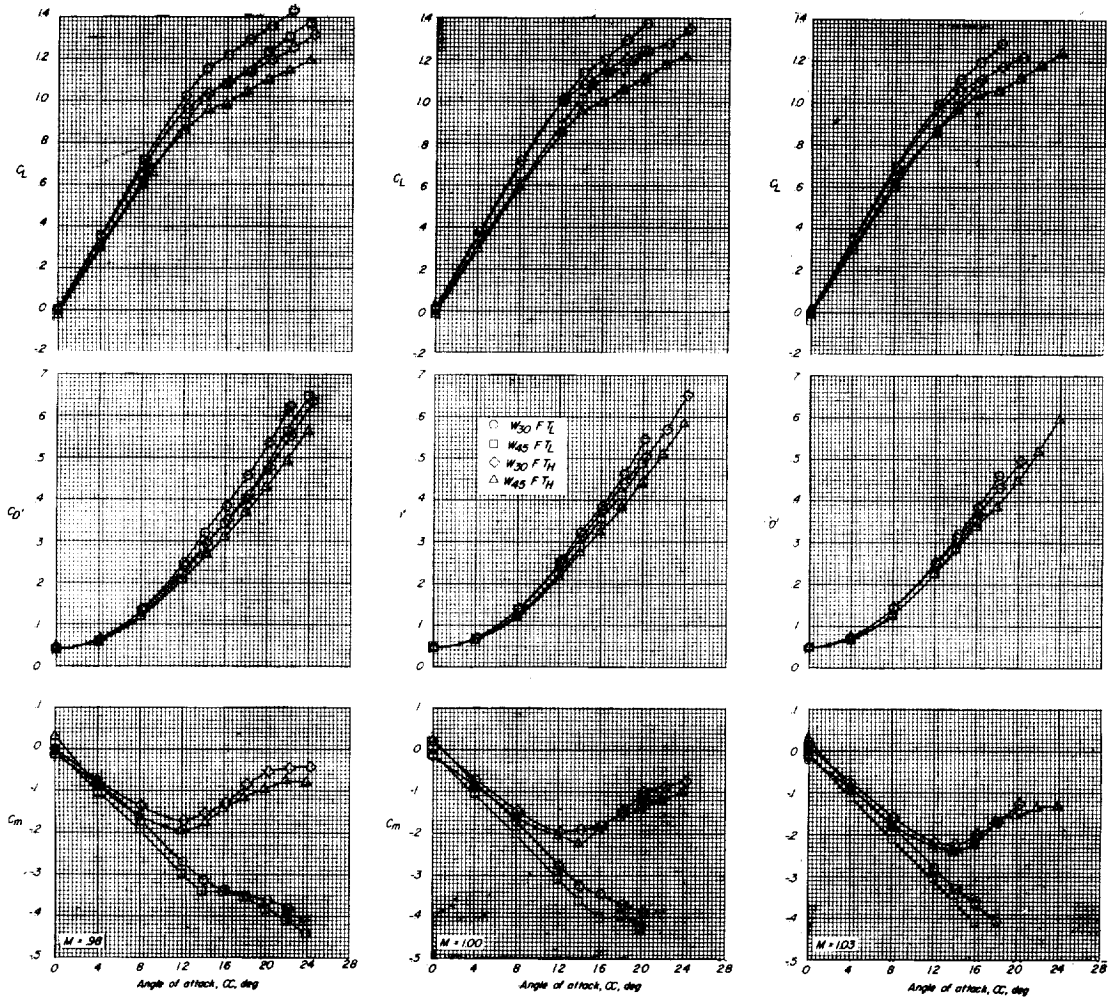

(d) M = 0.98. (e) M = 1.00. (f) M = 1.03.

Figure 5.- Continued.

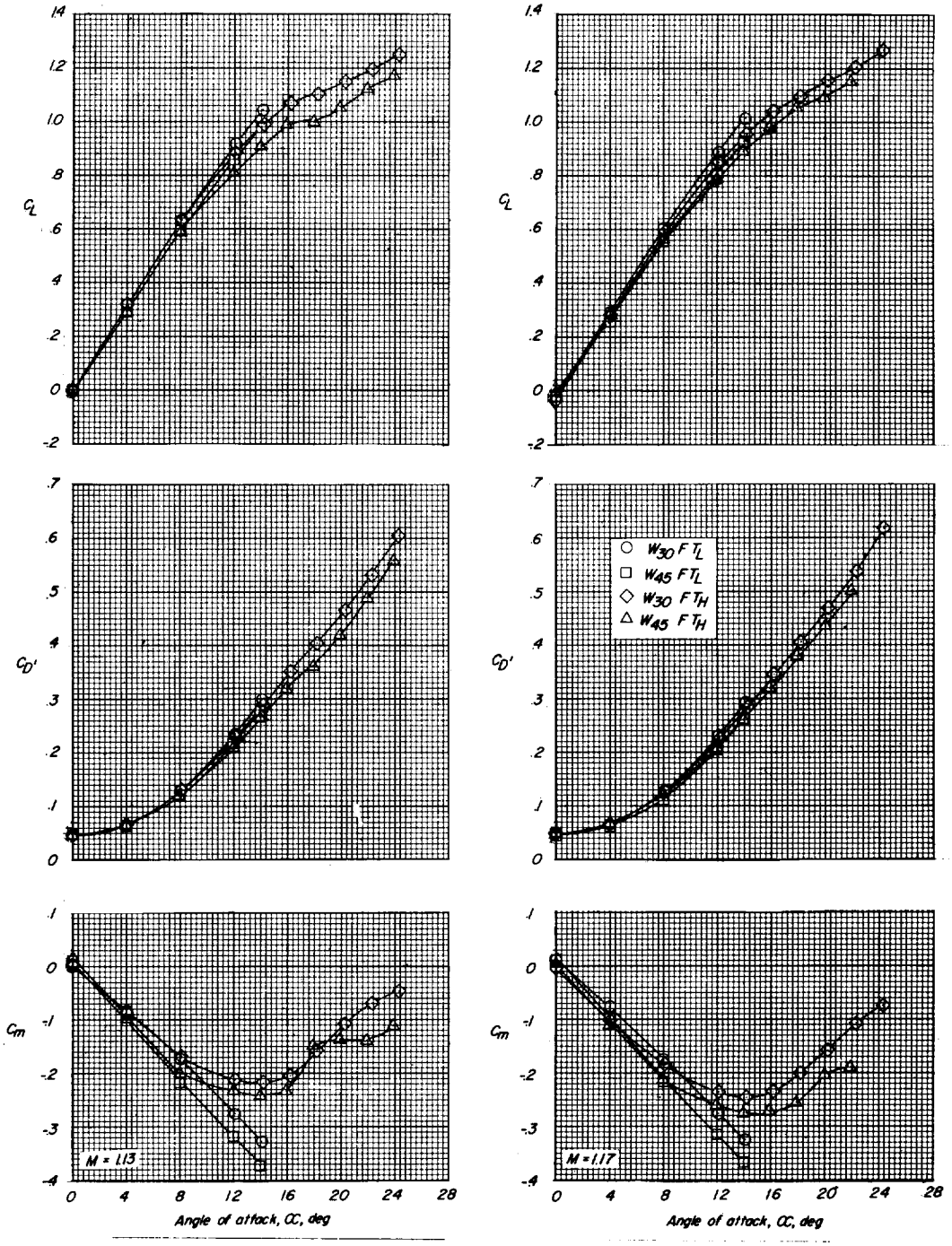

(g) M = 1.13. (h) M = 1.17.

Figure 5.- Concluded.

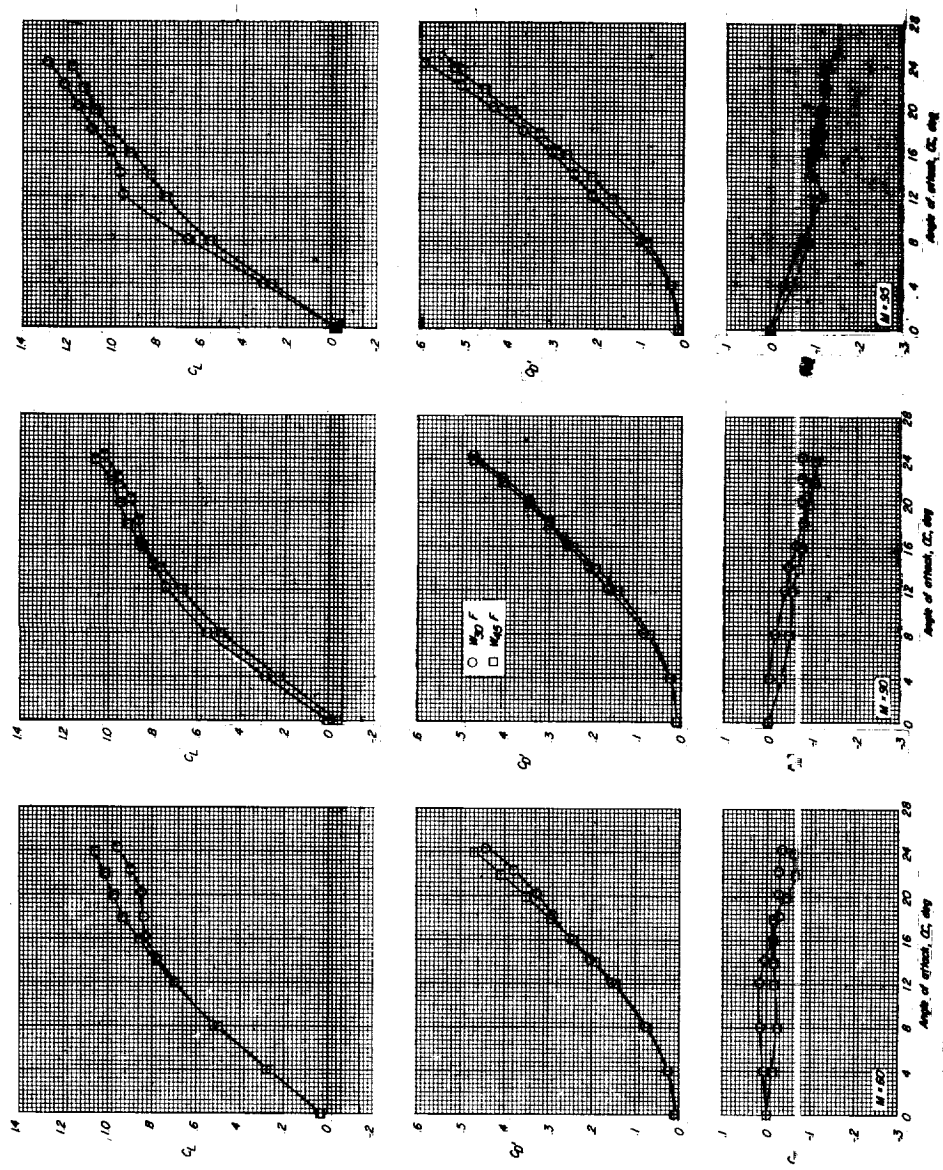

(a) M = 0.60. (b) M = 0.90. (c) M = 0.95.

Figure 6.- Variation with angle of attack of longitudinal aerodynamic coefficients for the model showing the effect of wing sweepback in the absence of the tail surfaces.

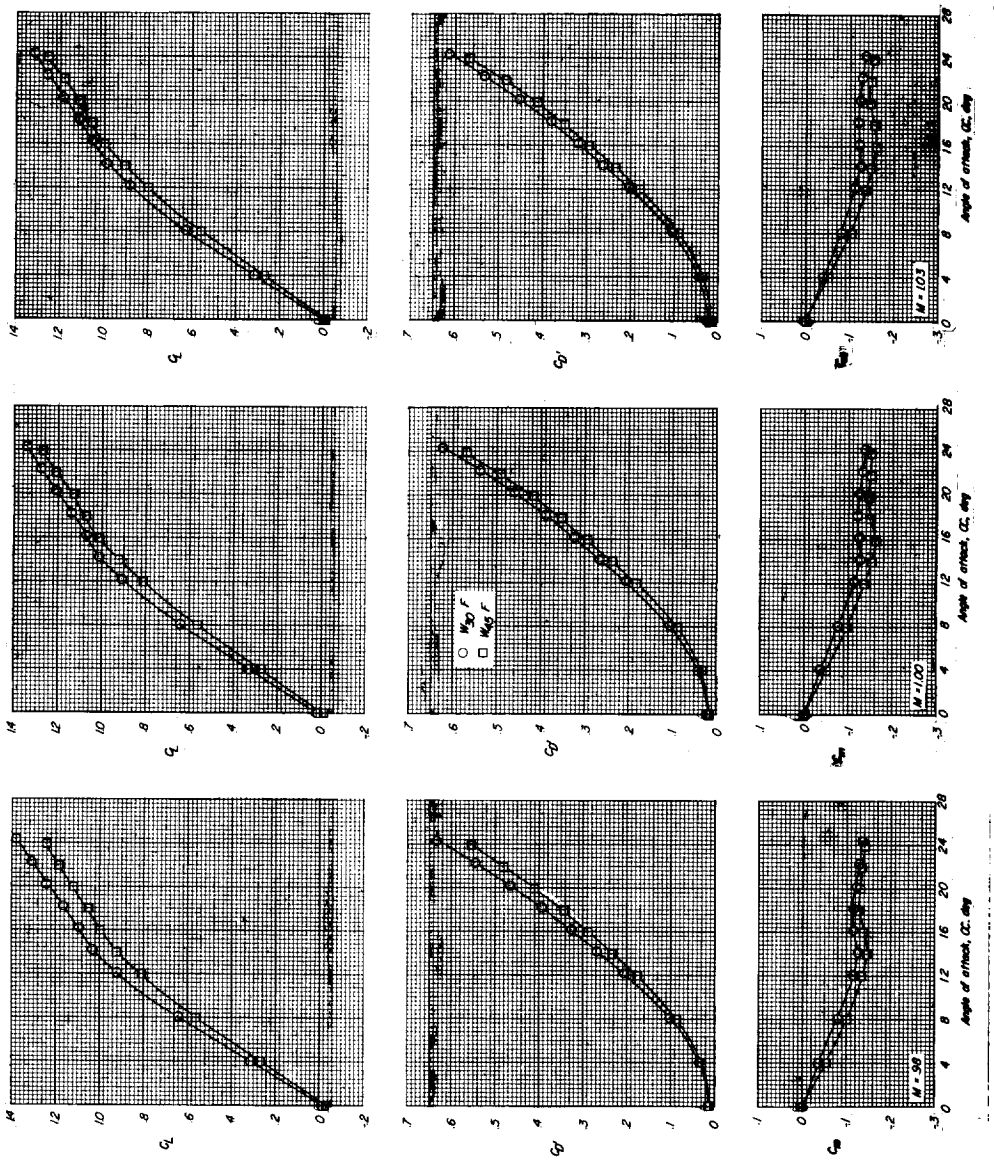

(d) M = 0.98. (e) M = 1.00. (f) M = 1.03.

Figure 6.- Continued.

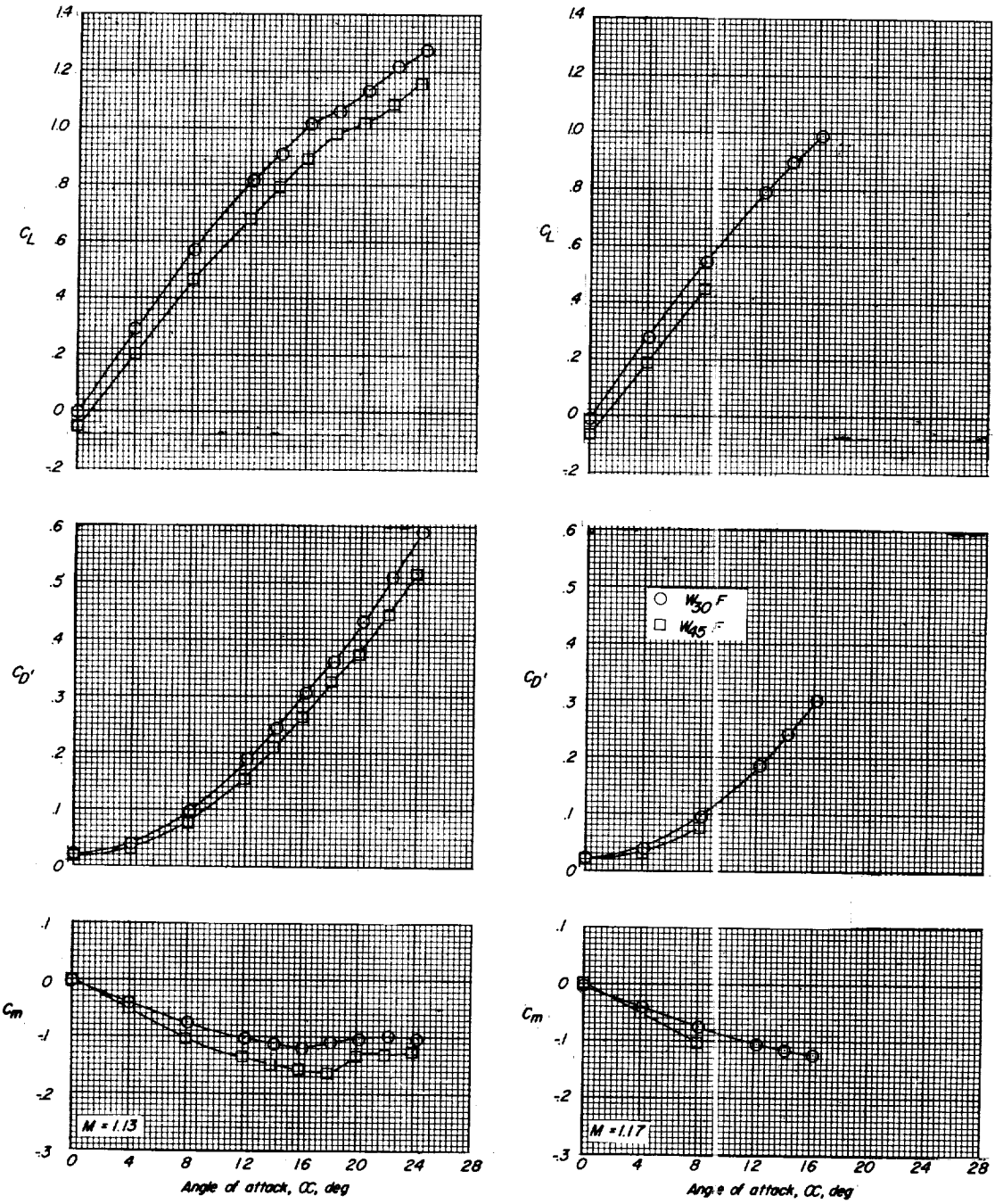

(g) M = 1.13. (h) M = 1.17.

Figure 6.- Concluded.

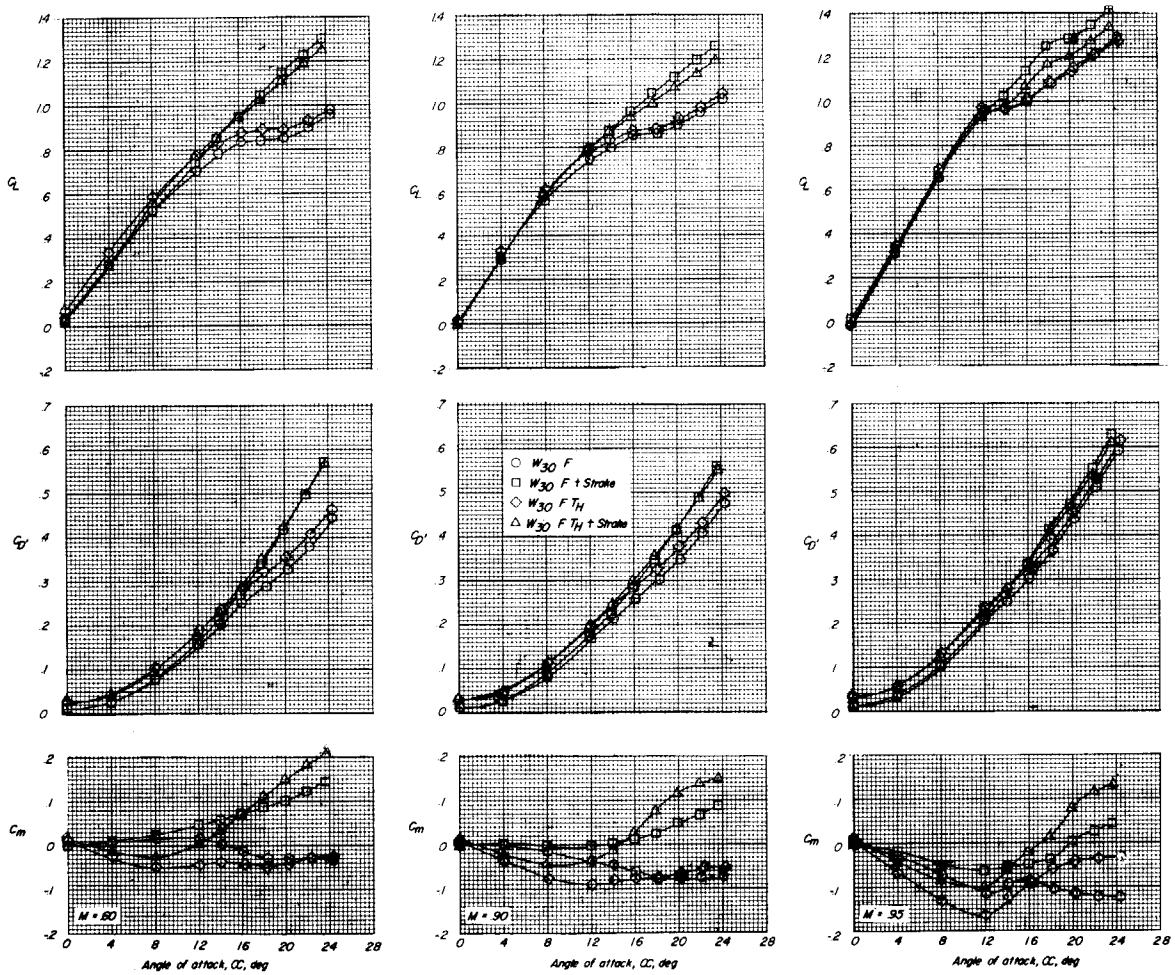

(a) M = 0.60. (b) M = 0.90. (c) M = 0.95.

Figure 7.- Effect of fuselage strakes on longitudinal coefficients for the model with the 30° sweptback wing, with the tails off, and with the horizontal tail in the high position.

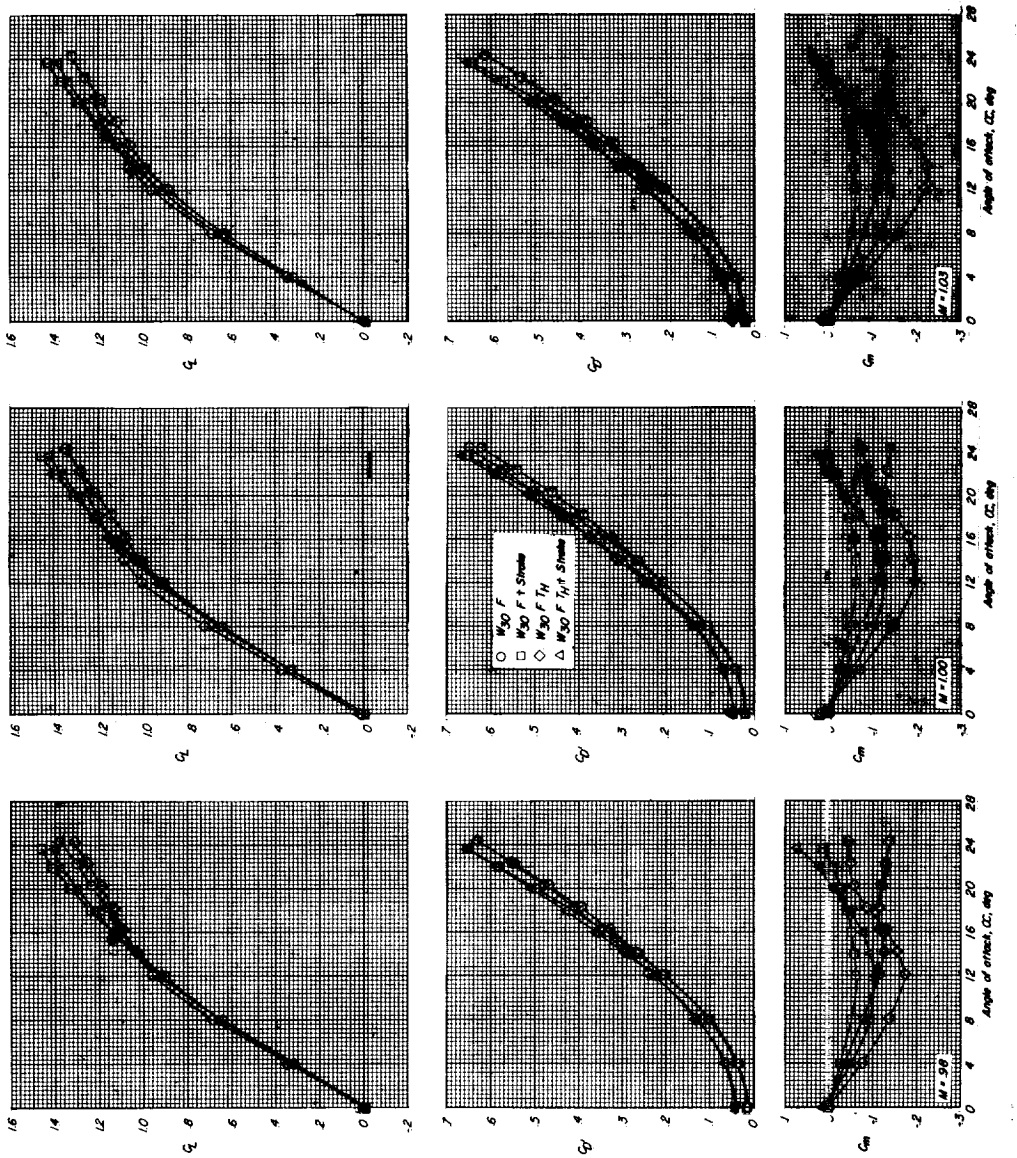

(d) M = 0.98. (e) M = 1.00. (f) M = 1.03.

Figure 7.- Continued.

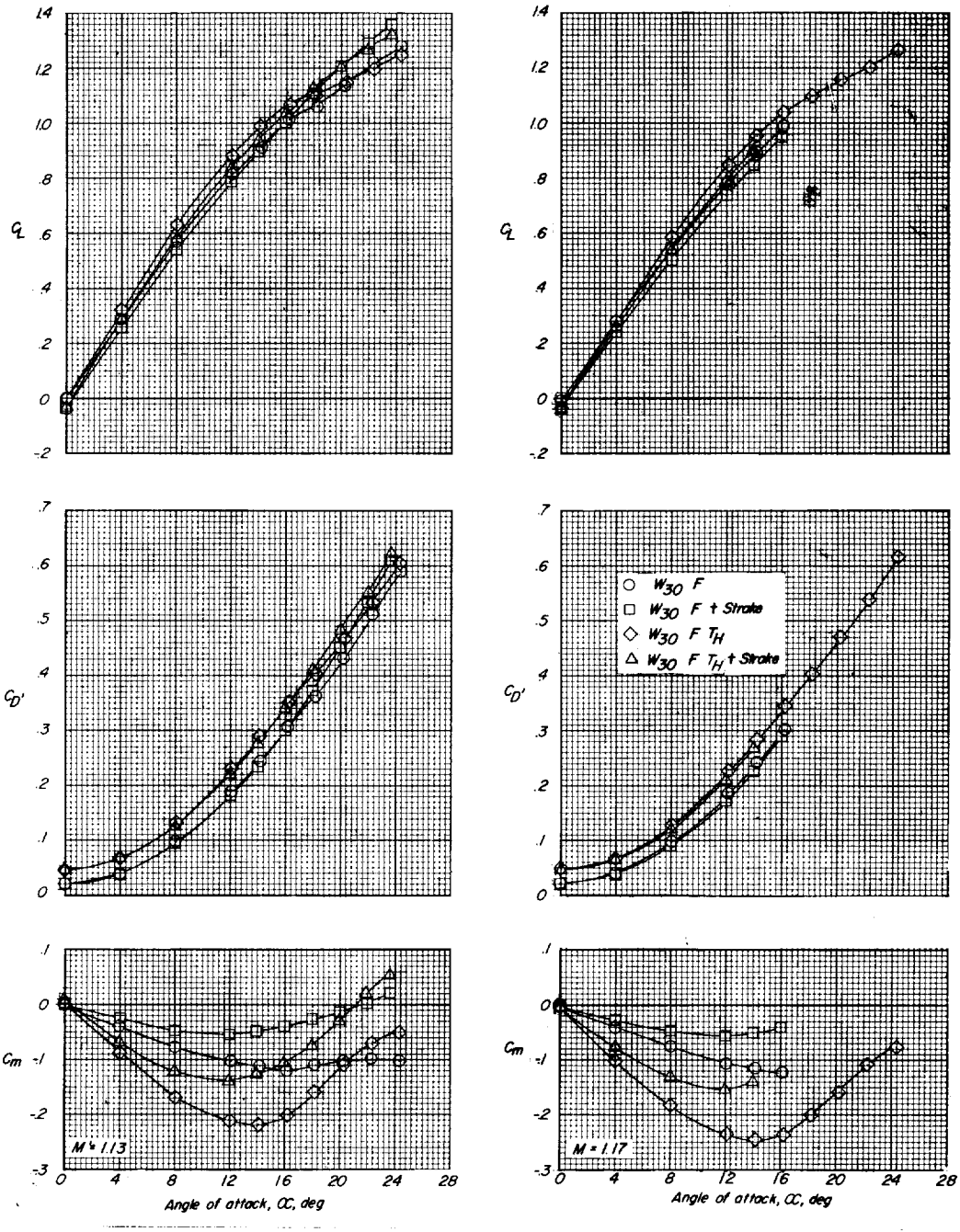

(g) M = 1.13. (h) M = 1.17.

Figure 7.- Concluded.

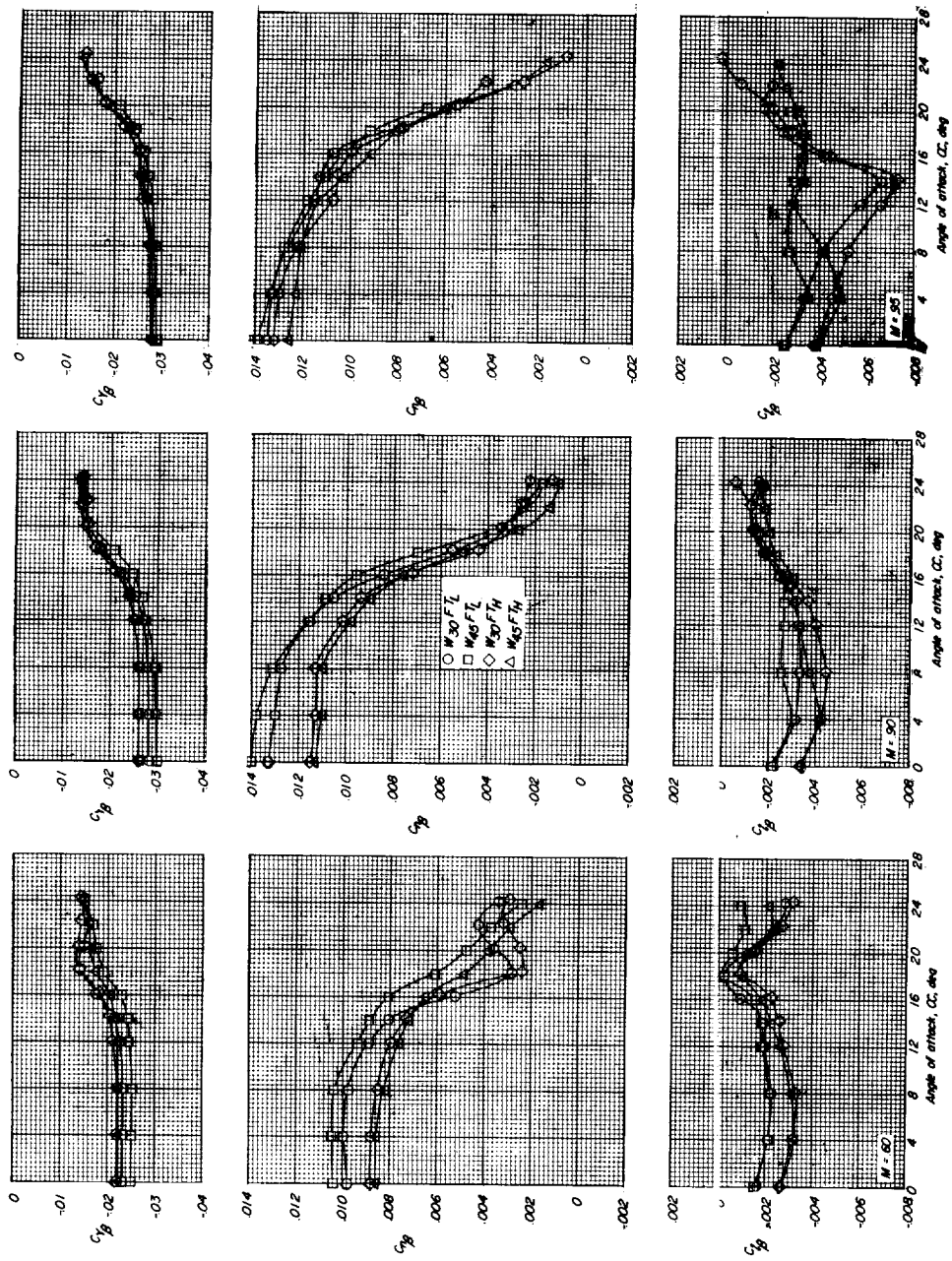

(a) M = 0.60. (b) M = 0.90. (c) M = 0.95.

Figure 8.- Effect of wing sweep and horizontal-tail height on lateral stability derivatives for the model.

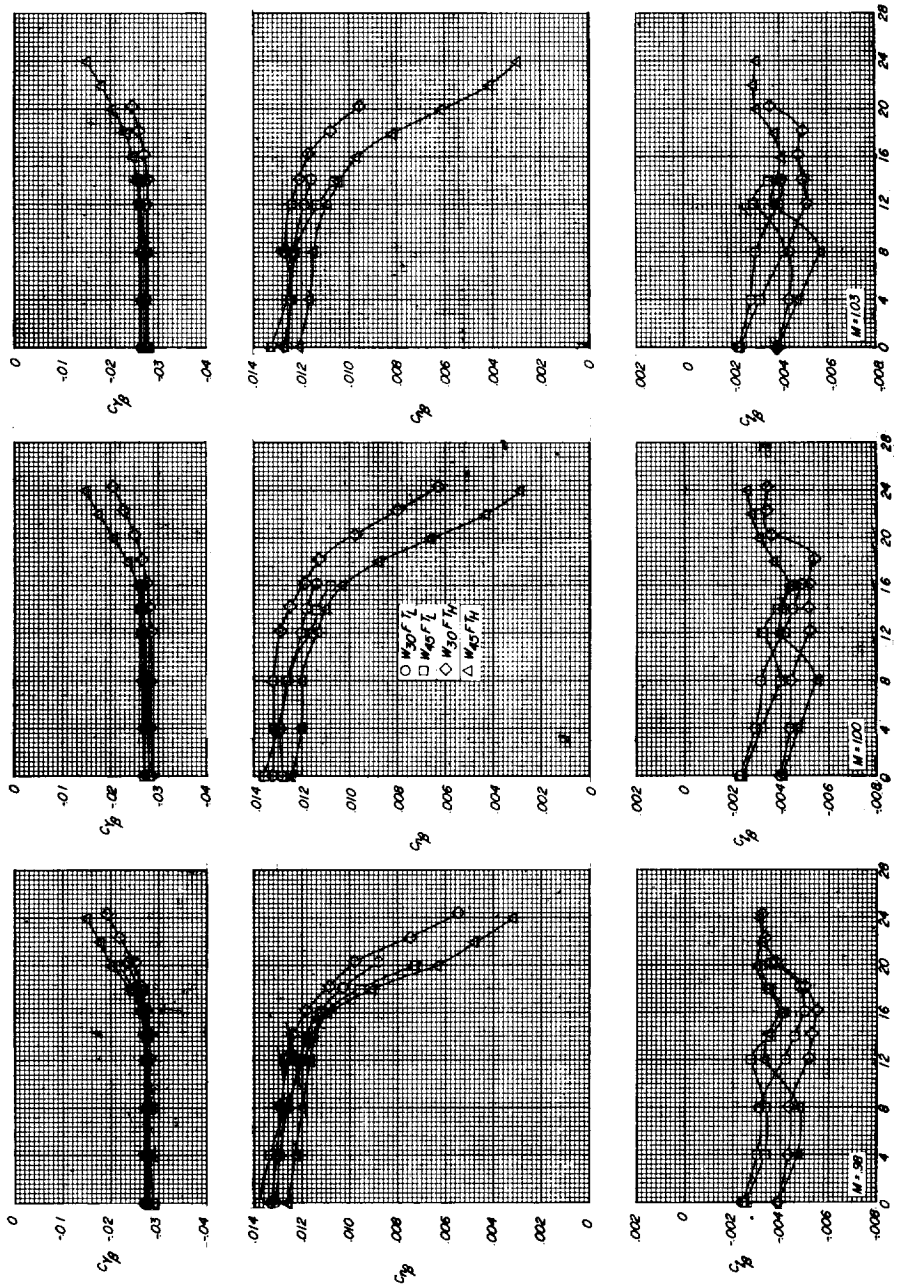

(d) M = 0.98. (e) M = 1.00. (f) M = 1.03.

Figure 8.- Continued.

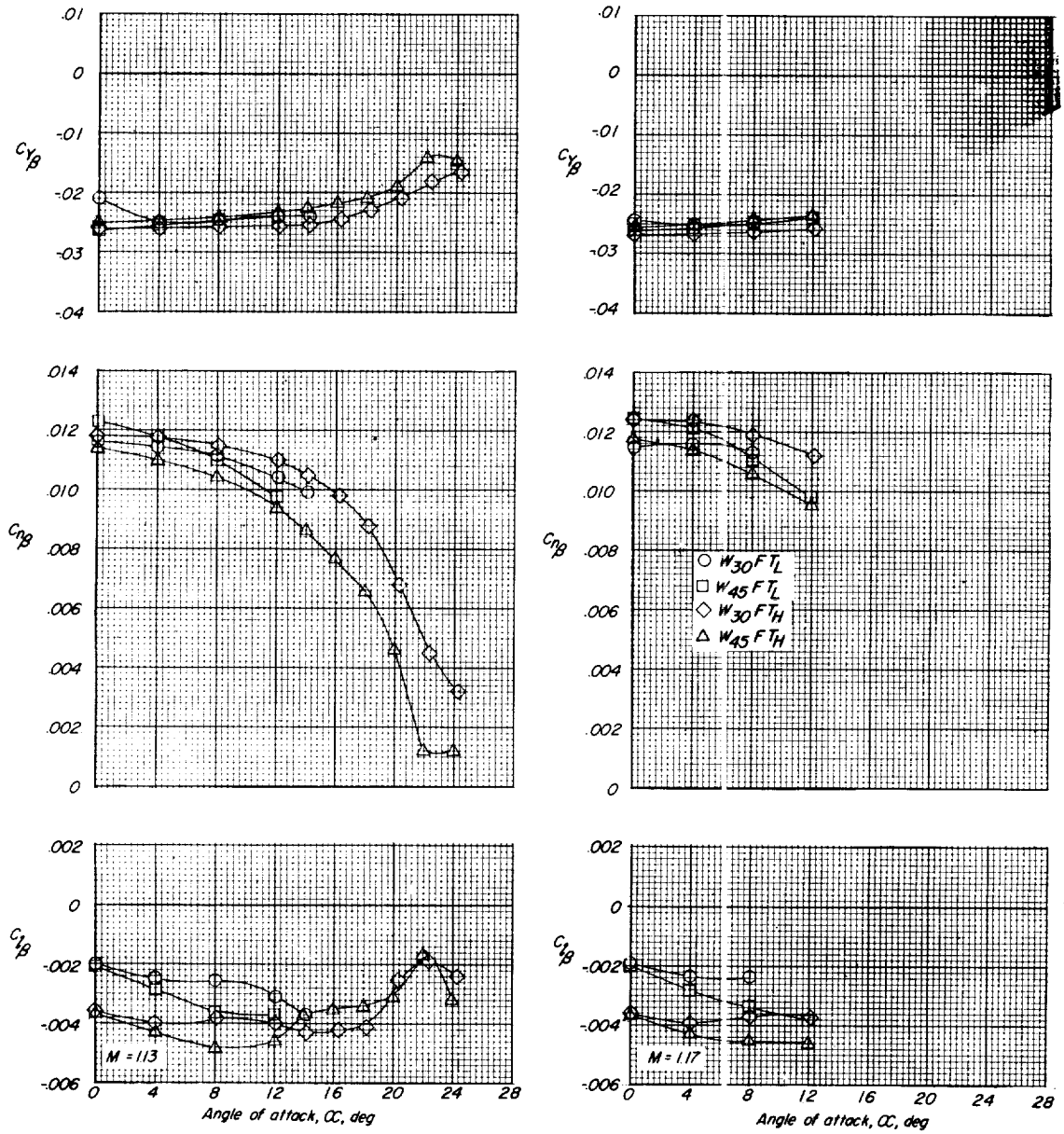

(g) M = 1.13.

(h) M = 1.17.

Figure 8.- Concluded.

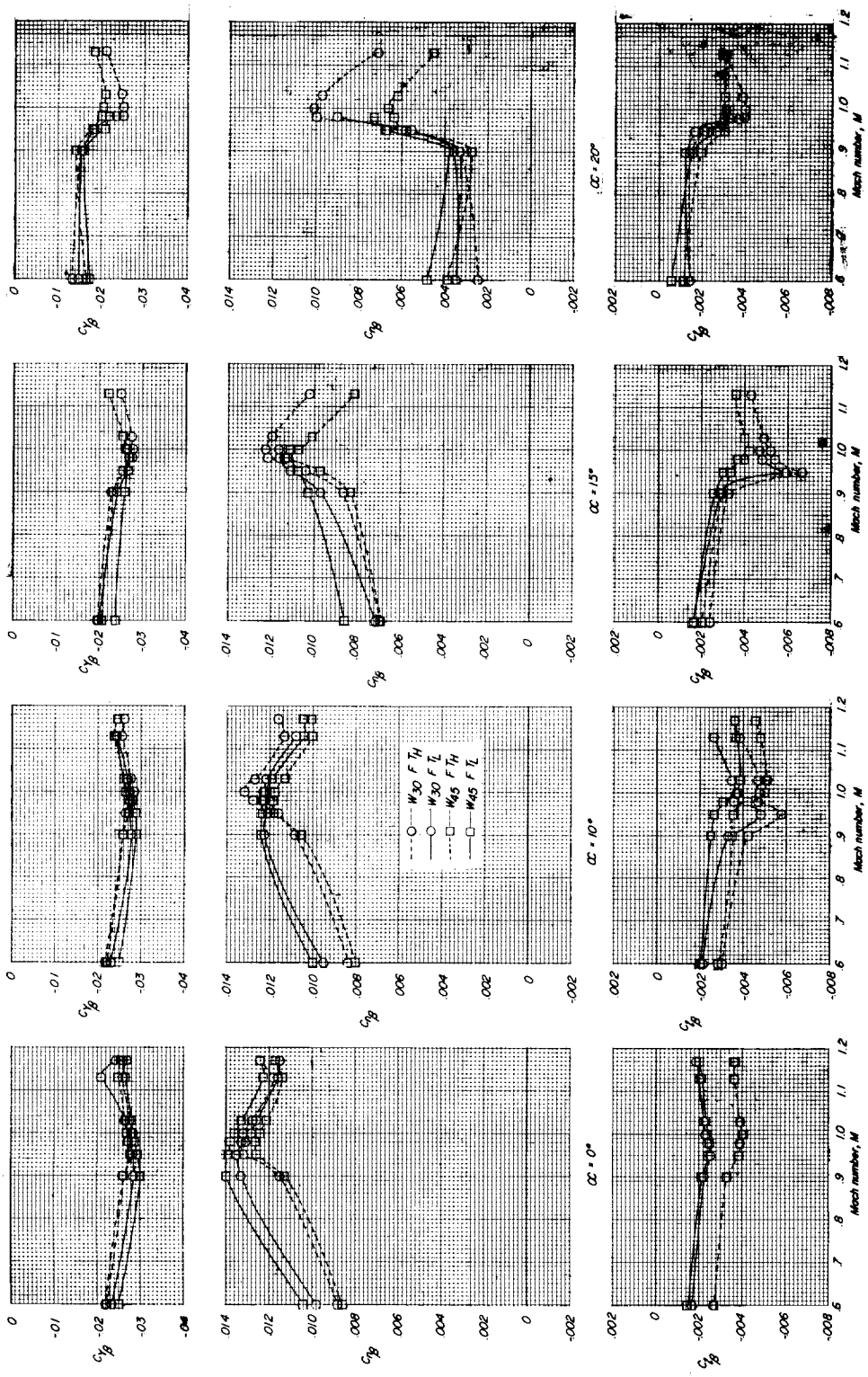

Figure 9.- Effect of Mach number on lateral stability derivatives for the model configurations tested for four angles of attack.

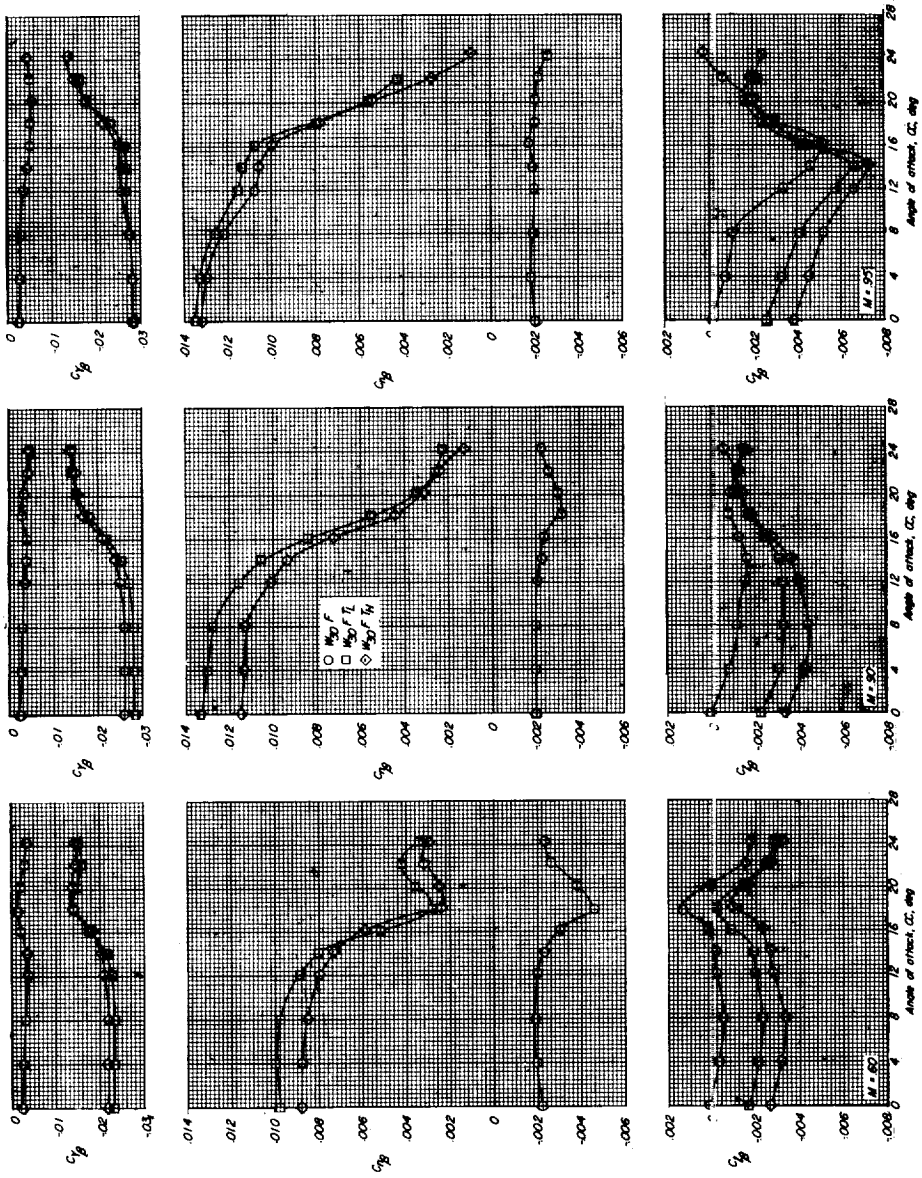

(a) M = 0.60. (b) M = 0.90. (c) M = 0.95.

Figure 10.- Effect of horizontal-tail height on lateral stability derivatives for the model with the 30° sweptback wing.

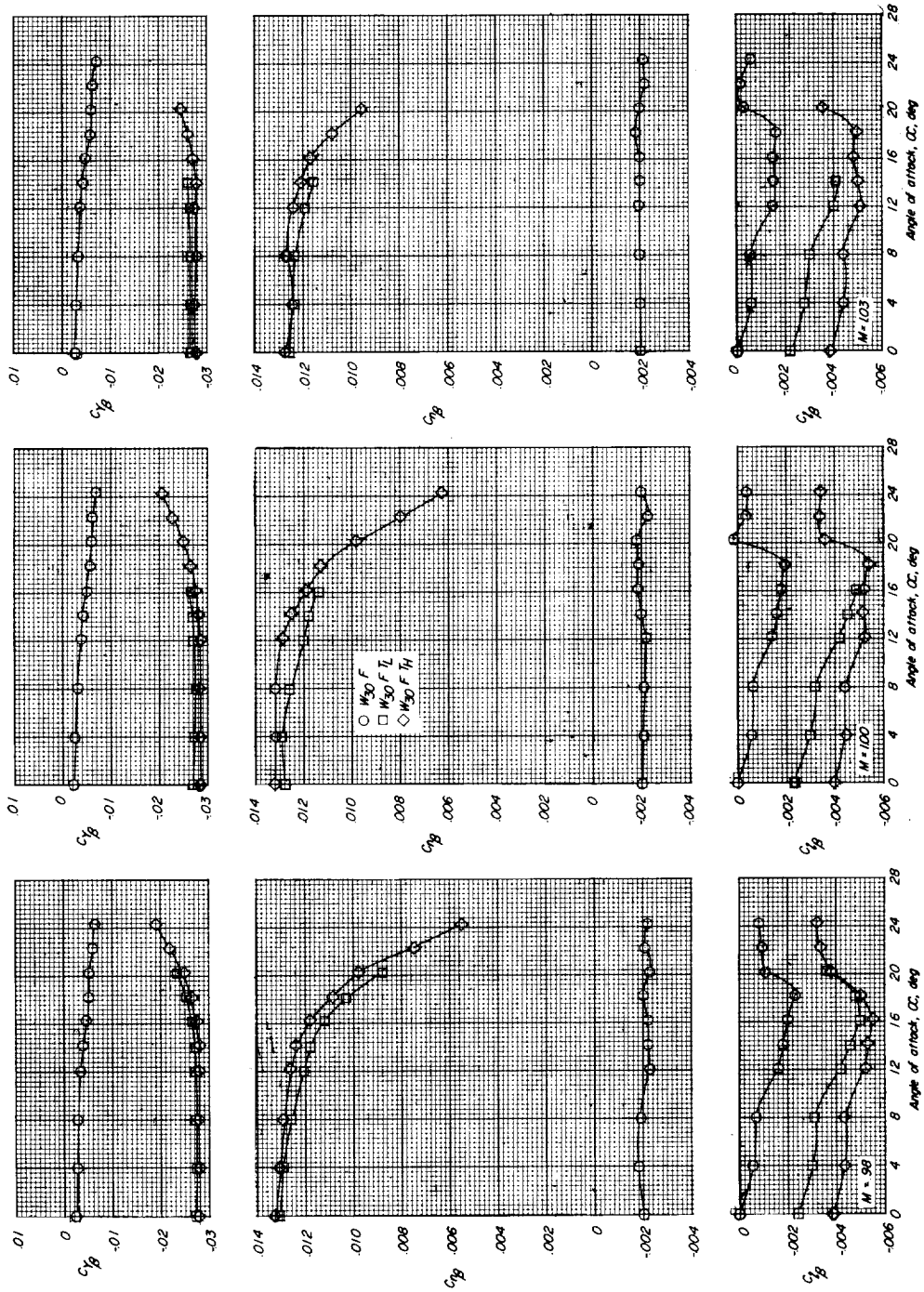

(d) M = 0.98. (e) M = 1.00. (f) M = 1.03.

Figure 10.- Continued.

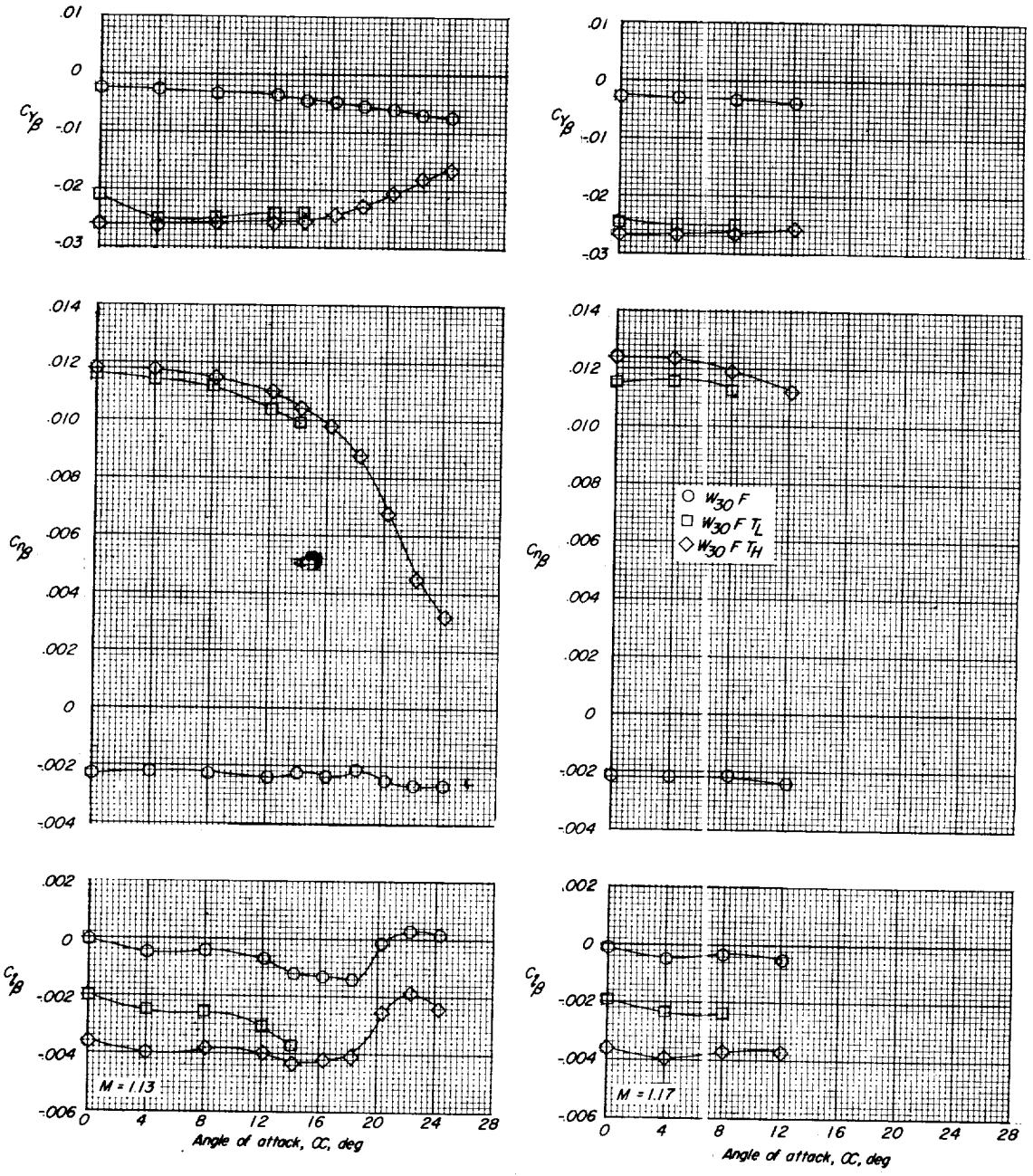

(g) M = 1.13.

(h) M = 1.17.

Figure 10.- Concluded.

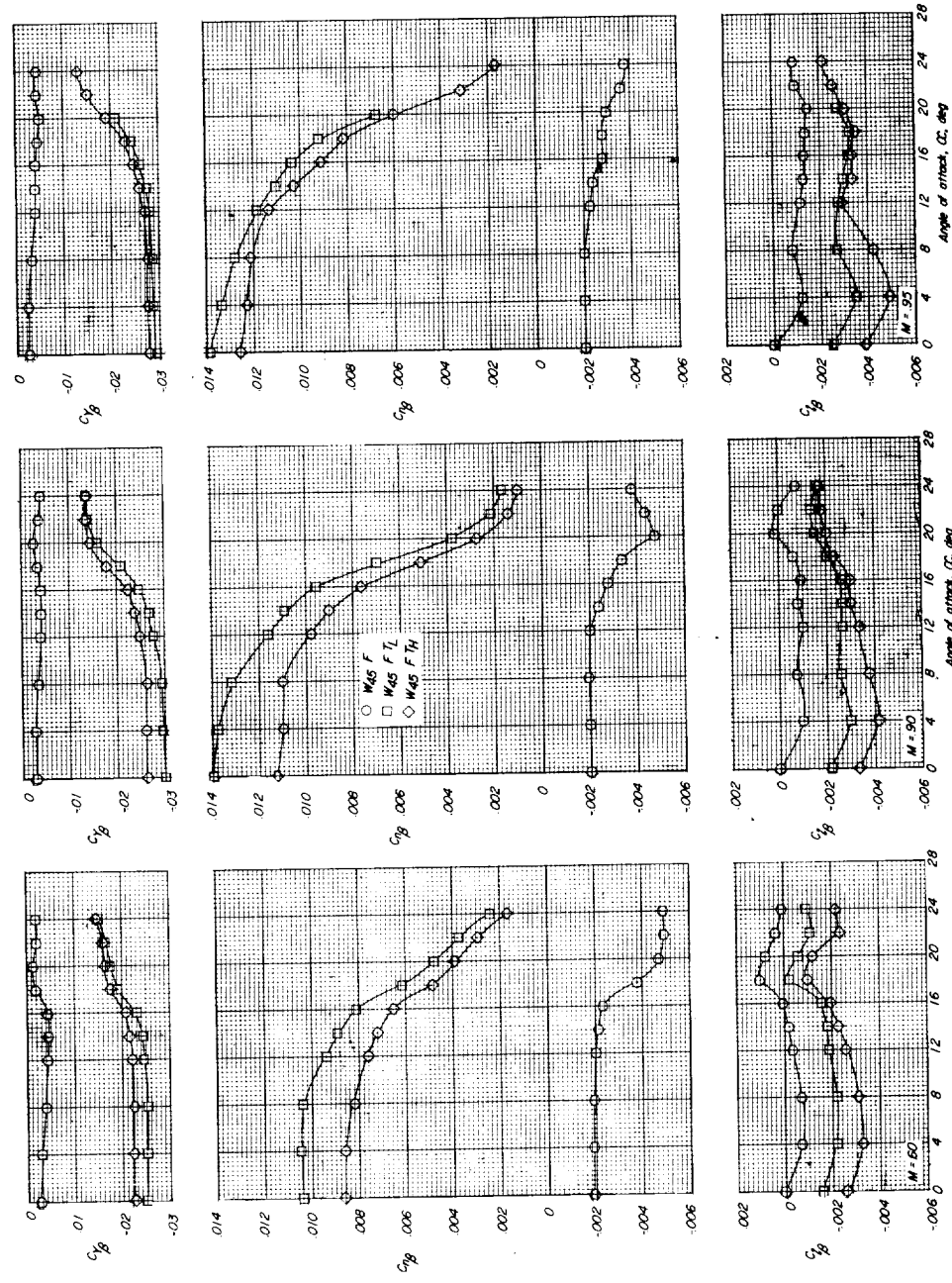

(a) M = 0.60. (b) M = 0.90. (c) M = 0.95.

Figure 11.- Effect of horizontal-tail height on lateral stability derivatives for the model with the 45° sweptback wing.

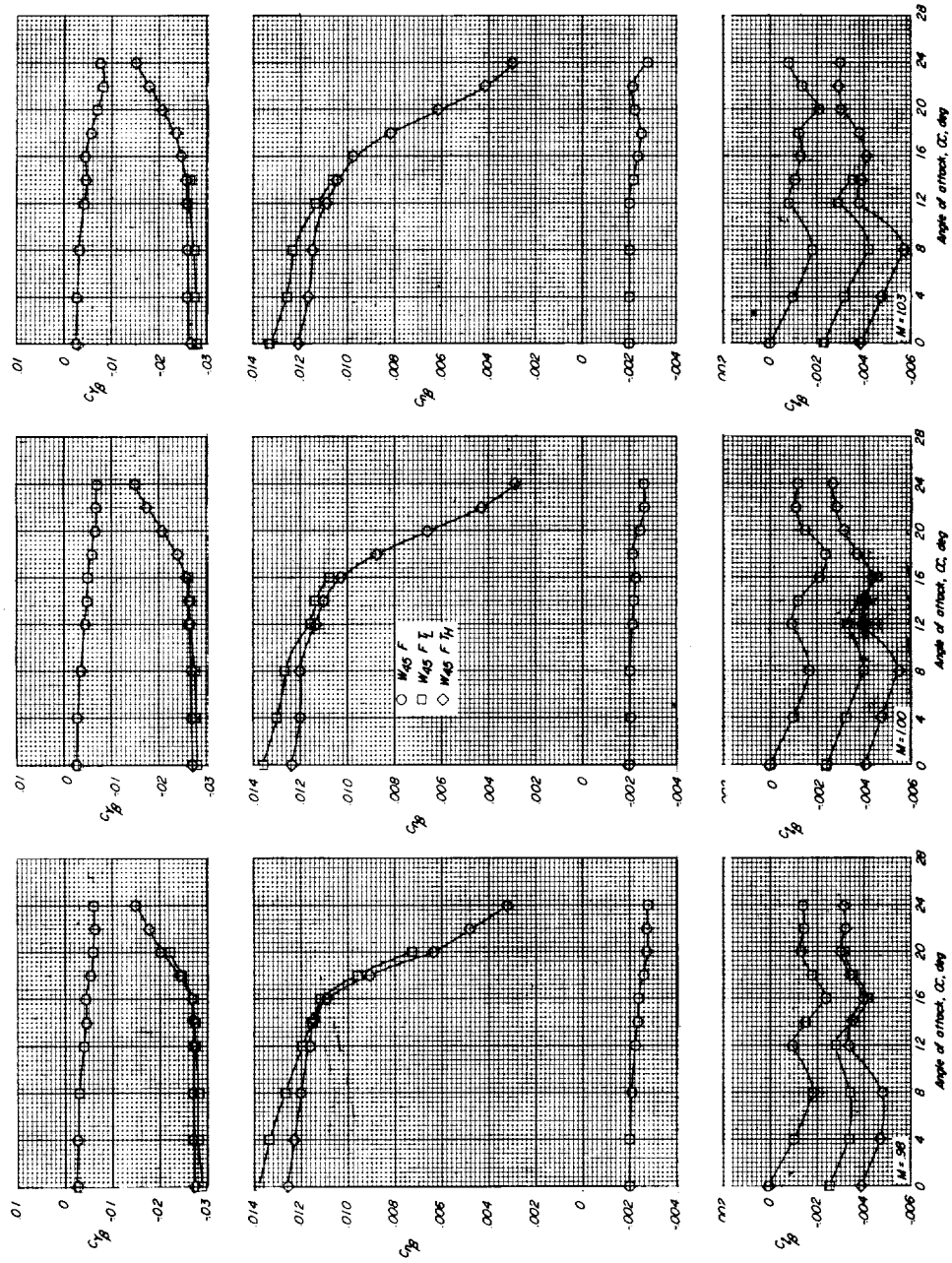

(d) M = 0.98. (e) M = 1.00. (f) M = 1.03.

Figure 11.- Continued.

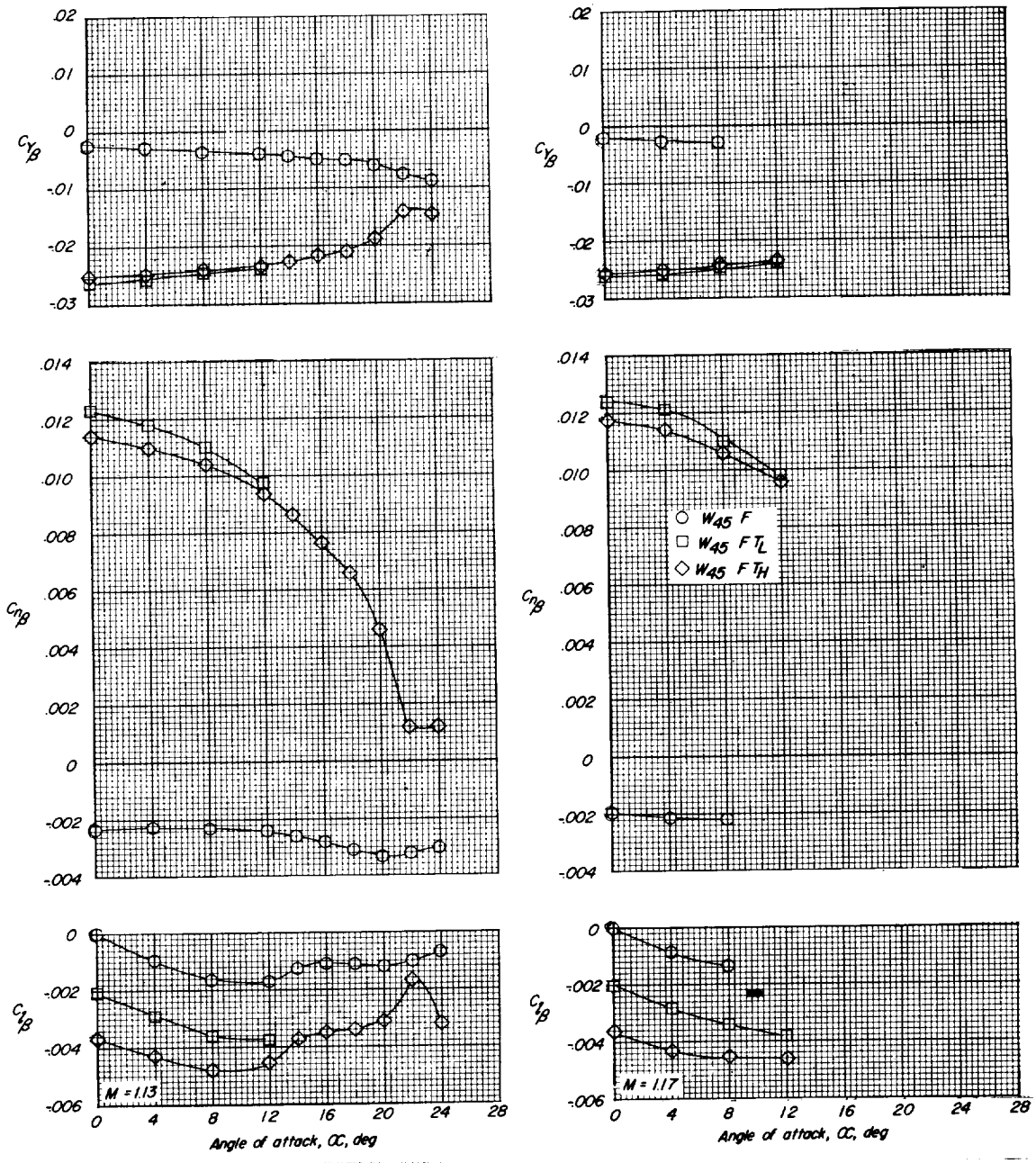

(g) M = 1.13. (h) M = 1.17.

Figure 11.- Concluded.

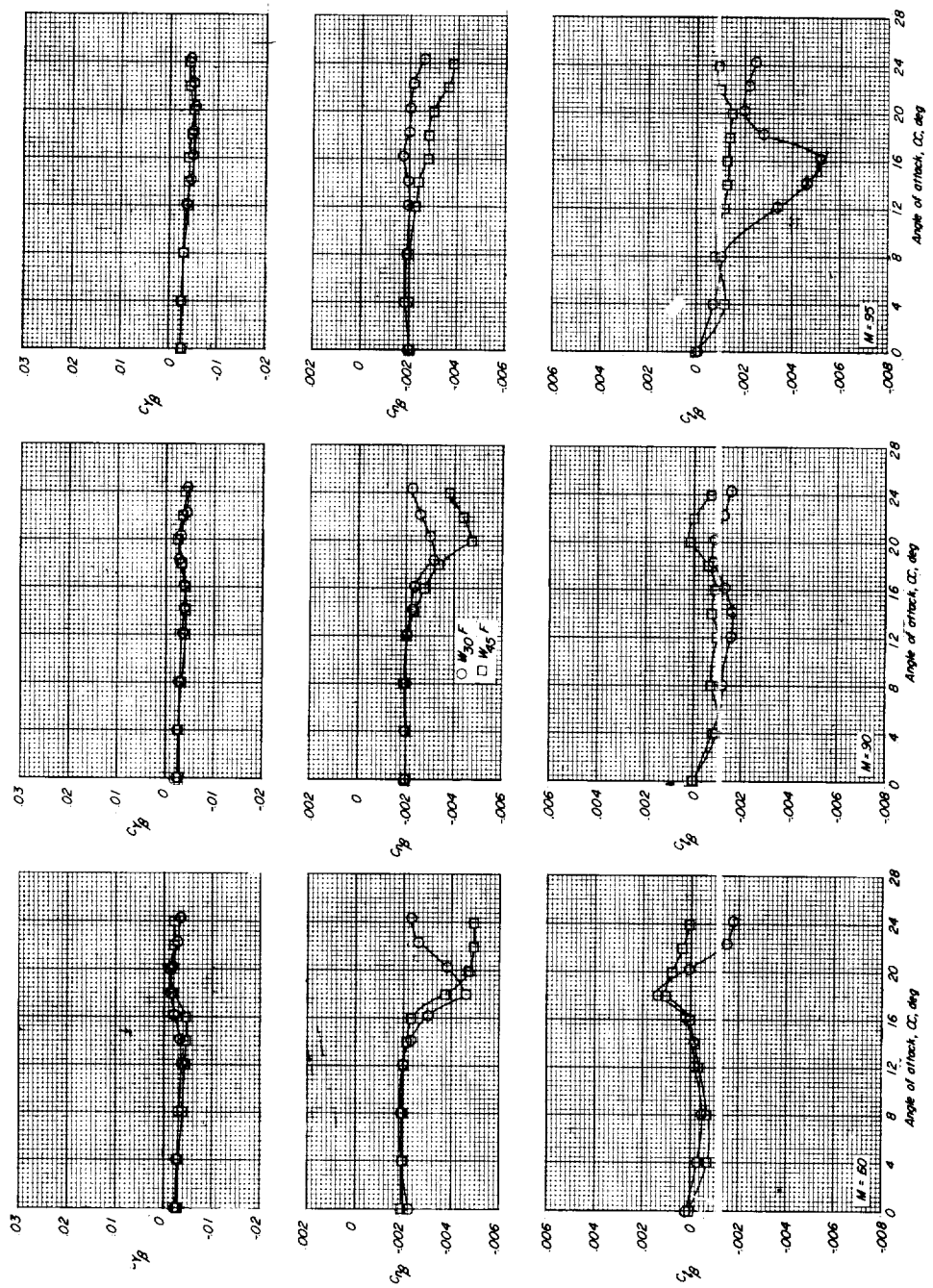

(a) M = 0.60. (b) M = 0.90. (c) M = 0.95.

Figure 12.- Effect of wing sweep on lateral stability derivatives for the model with no tail surfaces.

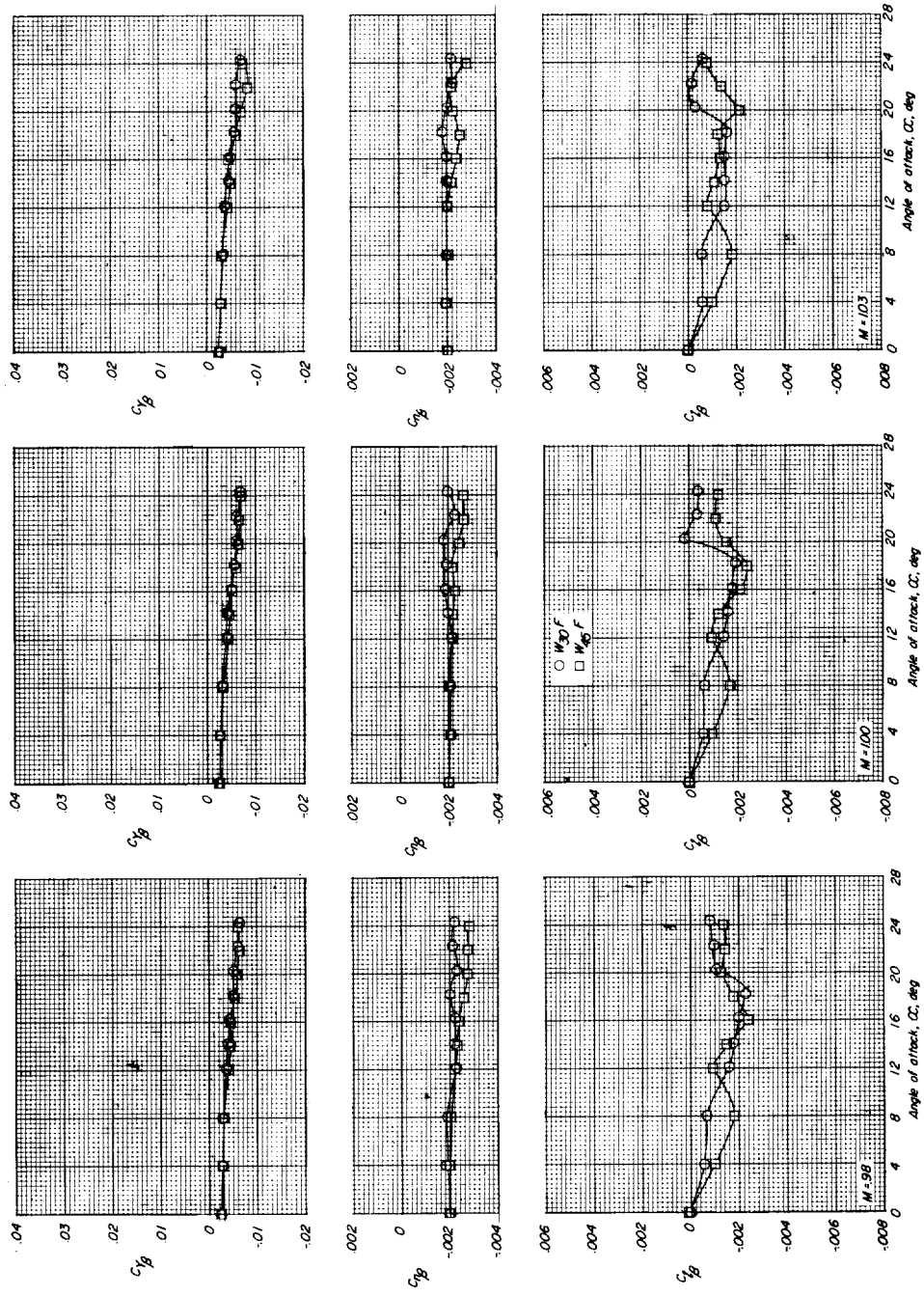

(d) M = 0.98. (e) M = 1.00. (f) M = 1.03.

Figure 12.- Continued.

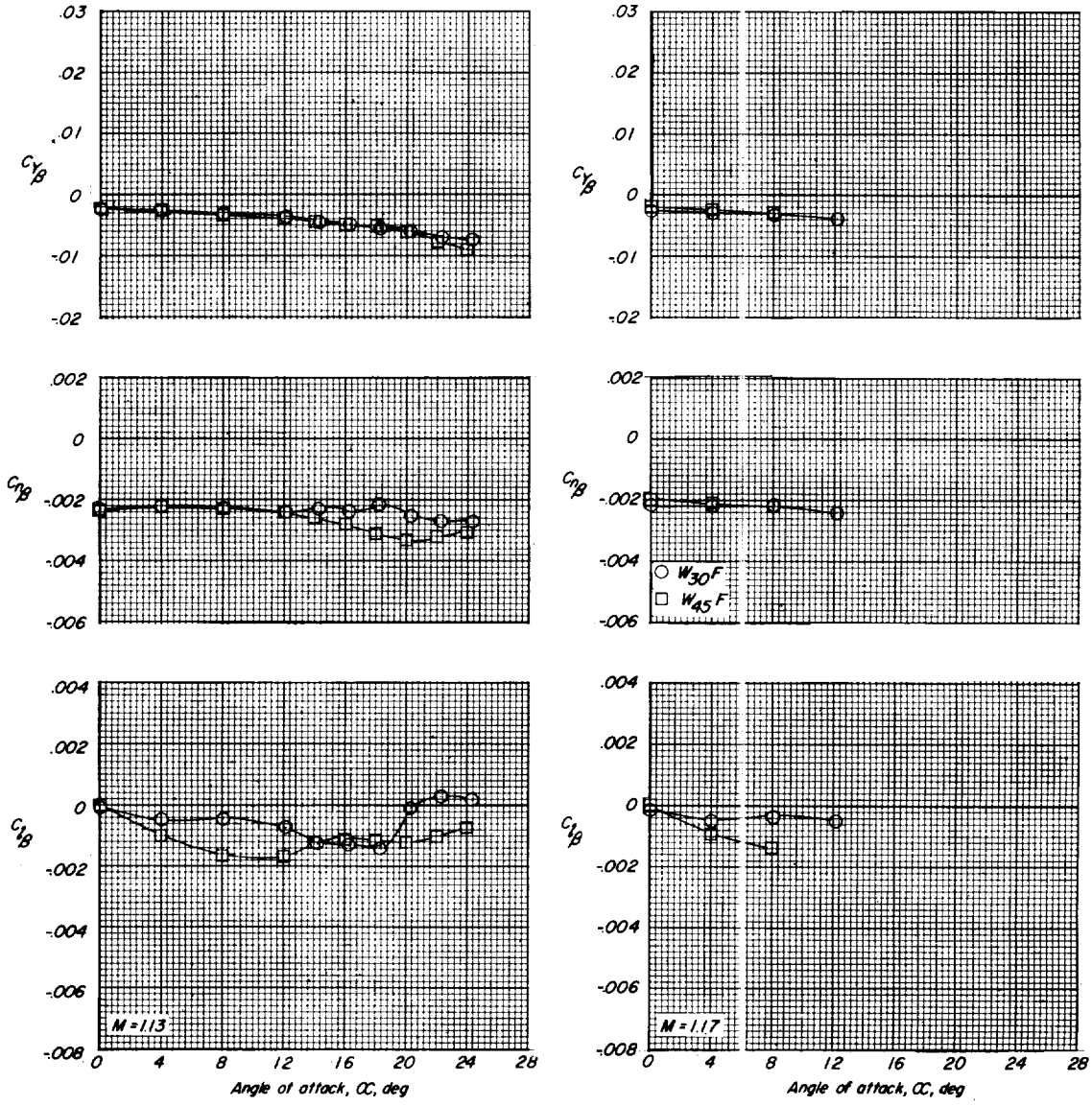

(g) M = 1.13. (h) M = 1.17.

Figure 12.- Concluded

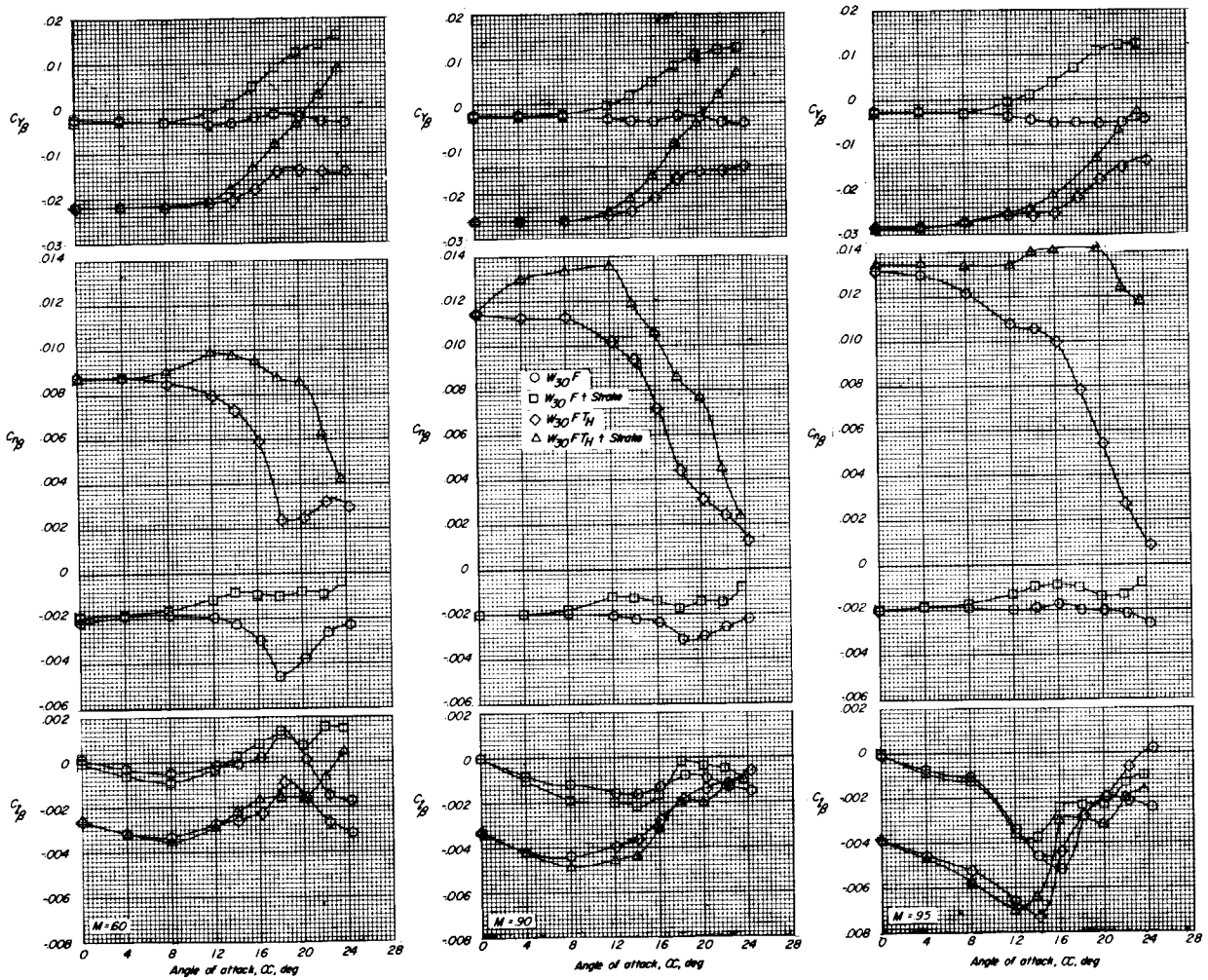

(a) M = 0.60. (b) M = 0.90. (c) M = 0.95.

Figure 13.- Effect of fuselage strakes on lateral stability derivatives for the 30°-sweptback-wing configuration with no tail surfaces and with the high horizontal-tail position.

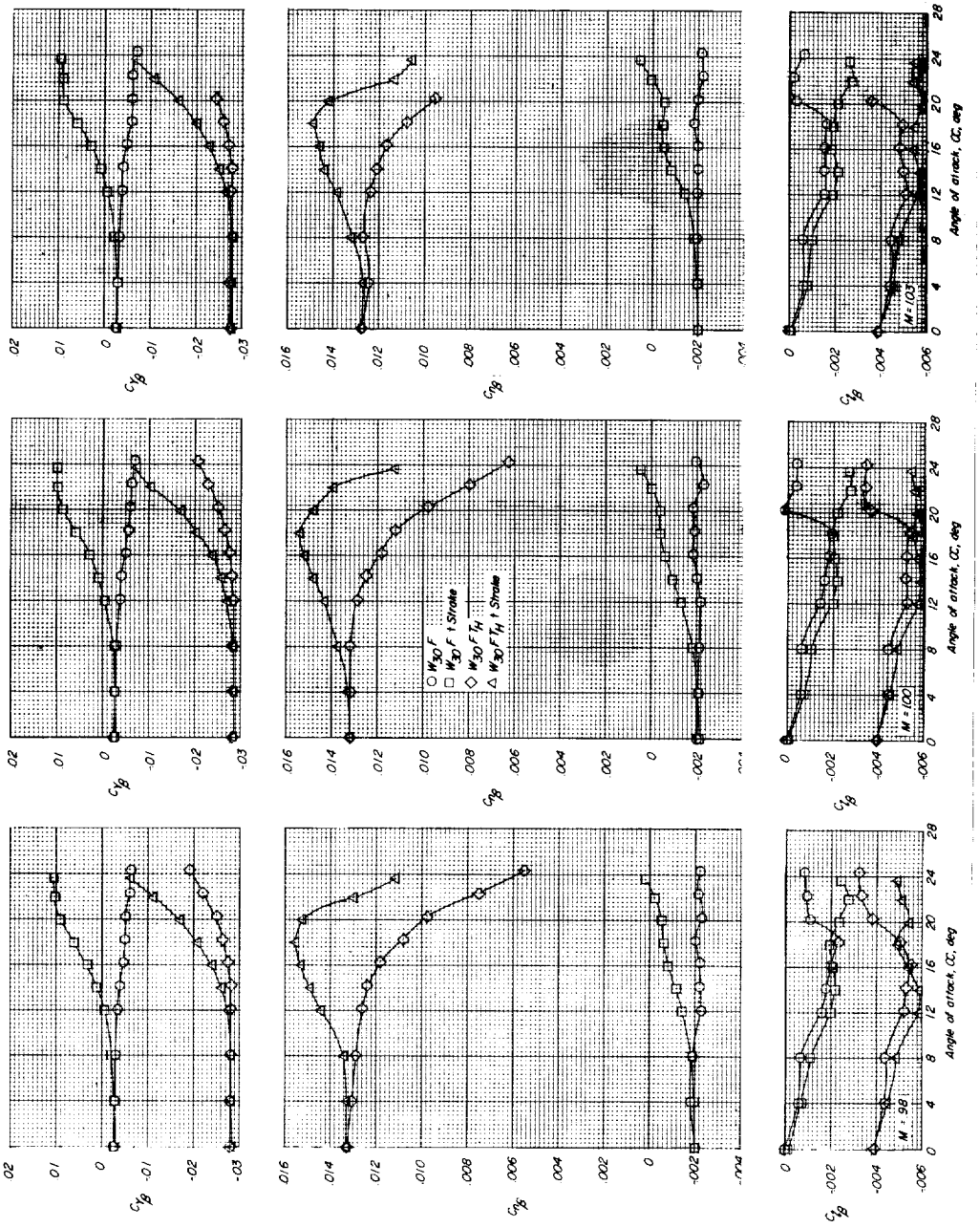

(a) M = 0.98. (e) M = 1.00. (f) M = 1.03.

Figure 13.- Continued.

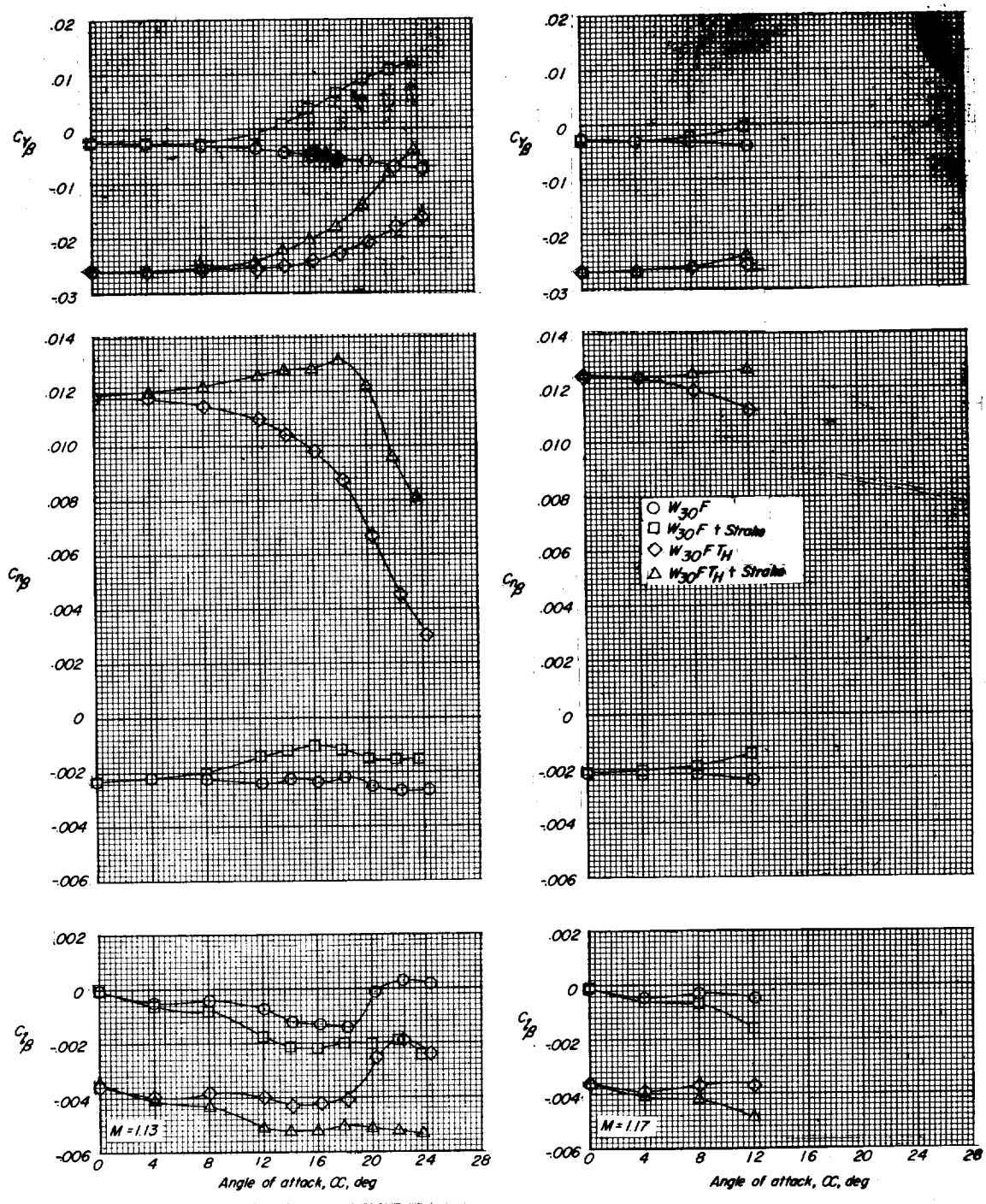

(g) M = 1.13. (h) M = 1.17.

Figure 13.- Concluded.

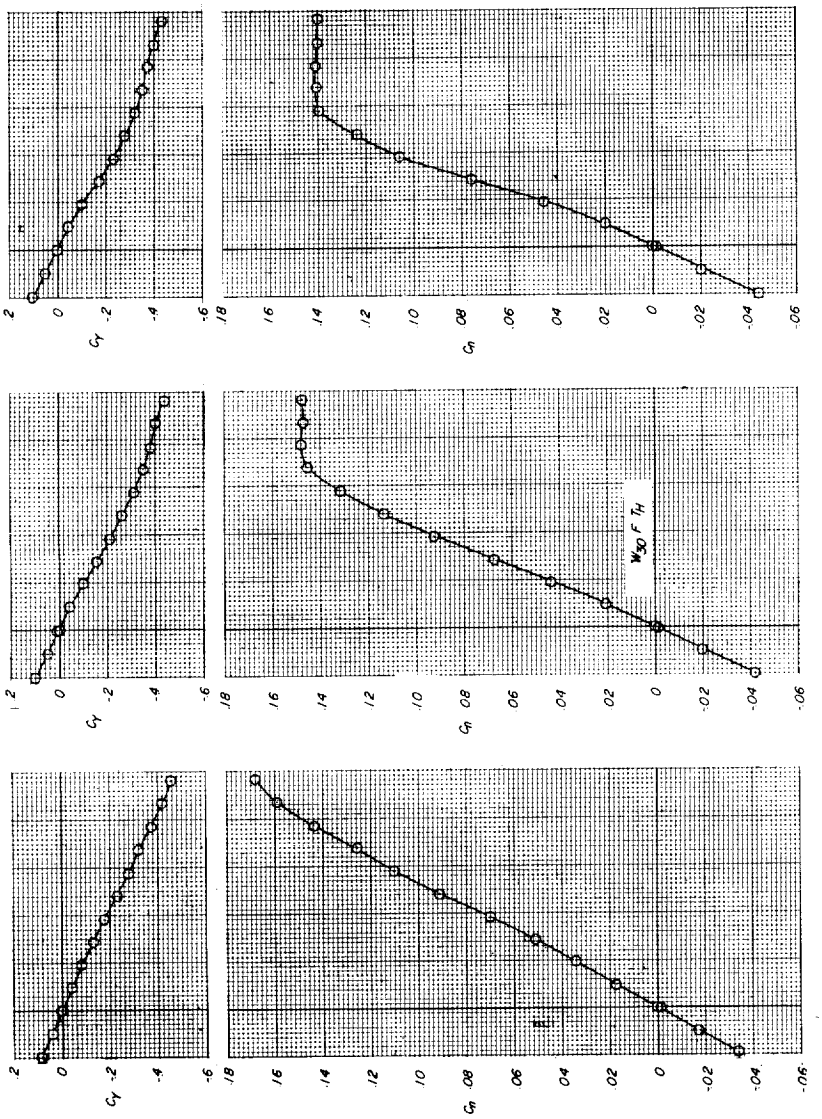

(a) M = 0.60. (b) M = 0.90. (c) M = 0.95.

Figure 14.- Representative variations of lateral coefficients with angle of sideslip for the 30°-sweptback-wing, high-horizontal-tail configuration. $\alpha = 6^{\circ}$.

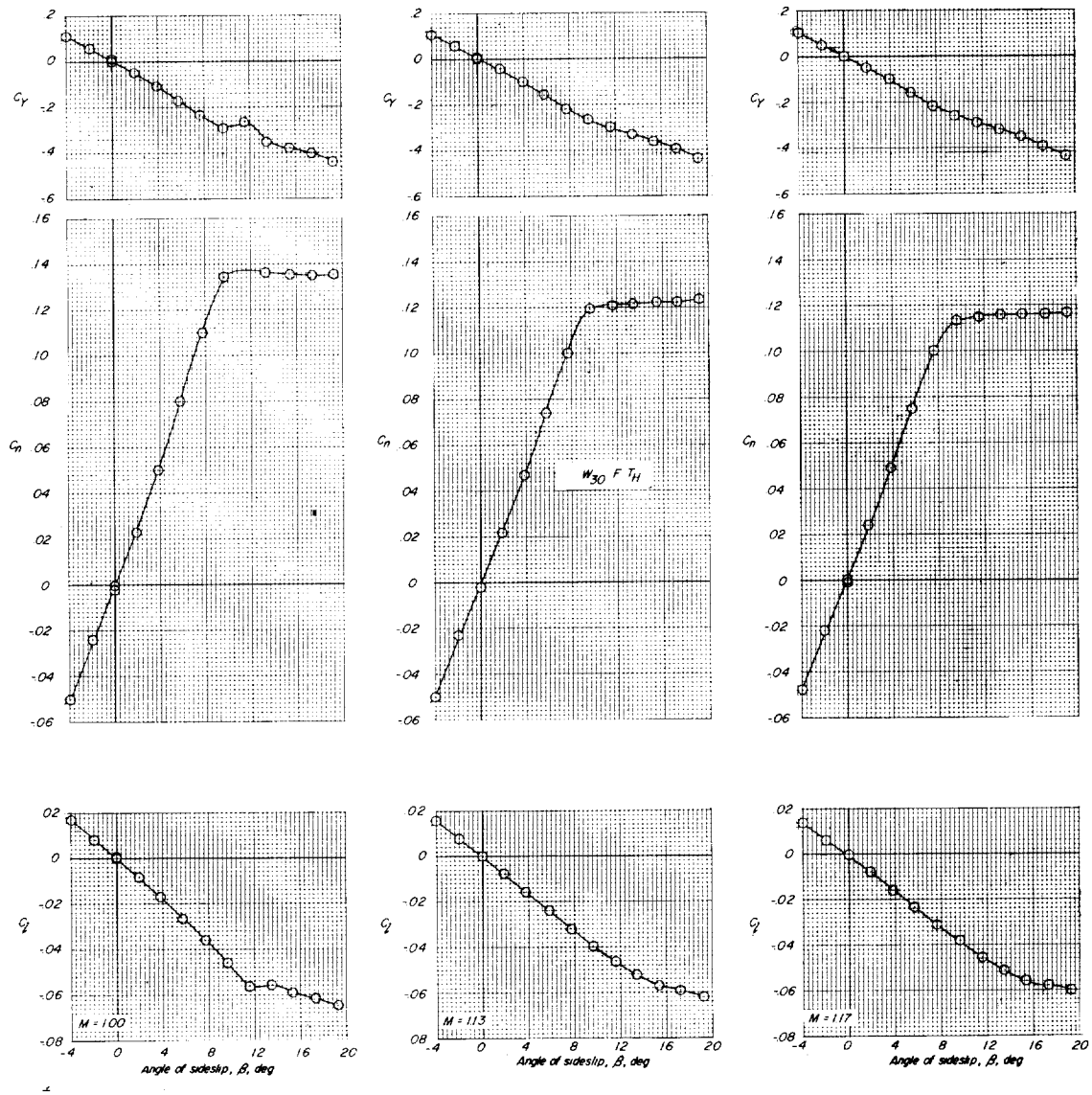

(d) M = 1.00. (e) M = 1.13. (f) M = 1.17.

Figure 14.- Concluded.